Future change of precipitation extremes in Europe: Intercomparison of scenarios from regional climate models

Christoph Frei,[1,2] Regina Schöll,[3] Sophie Fukutome,[4] Jürg Schmidli,[1] and Pier Luigi Vidale[5]

Received 11 March 2005; revised 1 October 2005; accepted 20 October 2005; published 24 March 2006.

[1] An analysis of the climate of precipitation extremes as simulated by six European regional climate models (RCMs) is undertaken in order to describe/quantify future changes and to examine/interpret differences between models. Each model has adopted boundary conditions from the same ensemble of global climate model integrations for present (1961–1990) and future (2071–2100) climate under the Intergovernmental Panel on Climate Change A2 emission scenario. The main diagnostics are multiyear return values of daily precipitation totals estimated from extreme value analysis. An evaluation of the RCMs against observations in the Alpine region shows that model biases for extremes are comparable to or even smaller than those for wet day intensity and mean precipitation. In winter, precipitation extremes tend to increase north of about 45°N, while there is an insignificant change or a decrease to the south. In northern Europe the 20-year return value of future climate corresponds to the 40- to 100-year return value of present climate. There is a good agreement between the RCMs, and the simulated change is similar to a scaling of present-day extremes by the change in average events. In contrast, there are large model differences in summer when RCM formulation contributes significantly to scenario uncertainty. The model differences are well explained by differences in the precipitation frequency and intensity process, but in all models, extremes increase more or decrease less than would be expected from the scaling of present-day extremes. There is evidence for a component of the change that affects extremes specifically and is consistent between models despite the large variation in the total response.

Citation: Frei, C., R. Schöll, S. Fukutome, J. Schmidli, and P. L. Vidale (2006), Future change of precipitation extremes in Europe: Intercomparison of scenarios from regional climate models, *J. Geophys. Res.*, *111*, D06105, doi:10.1029/2005JD005965.

1. Introduction

[2] An accumulating body of evidence suggests that the increase of atmospheric greenhouse gas concentrations could increase the frequency of heavy precipitation in many regions of the globe: Physical considerations imply that the sensitivity of heavy precipitation may be determined primarily by the change in the atmospheric moisture transport capacity (governed by the Clausius-Clapeyron relation) rather than the change in mean precipitation and evaporation [*Trenberth*, 1999; *Allen and Ingram*, 2002; *Trenberth et al.*, 2003]. The moistening of the atmosphere could result in progressively larger frequency increases at high precipitation intensities, and increases could even occur in regions where mean precipitation decreases [*Katz and Acero*, 1994; *Frei et al.*, 1998; *Groisman et al.*, 1999]. Consistent with these conceptual considerations, recent global warming experiments with general circulation models (GCMs) show an increase of precipitation extremes over many areas of the globe [e.g., *Kharin and Zwiers*, 2000; *Palmer and Räisänen*, 2002; *Semenov and Bengtsson*, 2002; *Voss et al.*, 2002; *Kiktev et al.*, 2003, 2004; *Watterson and Dix*, 2003; *Wehner*, 2004]. The details of the distribution and the magnitude of the change vary between models, but there is similarity in that increases are found predominantly over land areas of the middle and high latitudes.

[3] Results from GCMs may be considered with some reservation as regards the subcontinental pattern and magnitude of the change. The coarse grid spacing poses limitations to the explicit simulation of mesoscale processes and to the representation of topography and land-sea distribution. Regional climate models (RCMs) are promising tools, which, when nested into a GCM, permit the derivation of GCM-consistent climate change scenarios with more regional detail and a more trustworthy representation of processes active during heavy precipitation. Experiments

[1]Institute for Atmospheric and Climate Science, Eidgenössische Technische Hochschule, Zurich, Switzerland.
[2]Now at Federal Office of Meteorology and Climatology (MeteoSwiss), Zurich, Switzerland.
[3]Institute for Human-Environment Systems, Eidgenössische Technische Hochschule, Zurich, Switzerland.
[4]Institute of Terrestrial Ecology, Eidgenössische Technische Hochschule, Zurich, Switzerland.
[5]Center for Global Atmospheric Modelling, Department of Meteorology, University of Reading, Reading, UK.

0148-0227/06/2005JD005965$09.00

with the perfect model approach have demonstrated the ability of the one-way nesting technique in reproducing the fine-scale features of atmospheric fields in areas where surface forcing is strong [e.g., *Denis et al.*, 2002; *De Elia and Laprise*, 2003]. Also, RCMs were found to reproduce the main characteristics of the larger-scale hydroclimate during episodes of heavy precipitation [*Anderson et al.*, 2003] and prominent patterns of precipitation extremes on scales not resolved by a current GCM [*Frei et al.*, 2003; *Fowler et al.*, 2005]. However, biases are quite large in some cases. Note that there are alternative approaches to climate change downscaling using statistical techniques [e.g., *Wilby et al.*, 1998; C. M. Goodess et al., An intercomparison of statistical downscaling methods for Europe and European regions—Assessing their performance with respect to extreme temperature and precipitation events, submitted to *Climatic Change*, 2005], but we focus on dynamical downscaling, i.e., RCMs, in this study.

[4] For the European continent, a number of recent climate change simulations with regional climate models have been analyzed for future changes in precipitation extremes. One group of studies considers direct empirical diagnostics such as quantiles or seasonal/annual extremes; for example, *Durman et al.* [2001] found that the fraction of precipitation exceeding the 99th percentile of daily values increases in their RCM by several tens of percent by the end of the 21st century under a 1% per year CO_2 increase. In a different RCM, *Christensen and Christensen* [2003, 2004] found an increase of very high quantiles even in summer and for regions in central Europe, where mean precipitation decreases. *Pal et al.* [2004] found similar results in their RCM. *Räisänen et al.* [2004] documented an increase in annual precipitation extremes for two RCM experiments with different GCMs, but details of the geographical pattern of the change were different between the two experiments.

[5] Another group of studies has adopted techniques of extreme value analysis to estimate the change in events with return periods of several years. Using data from two RCMs, *Booij* [2002] estimated a 25–60% increase (depending on model) in the 20-year return period 1-day rainfall in an area of northwestern continental Europe by the time of CO_2 doubling. For the area of the United Kingdom, several applications of extreme value statistics have been undertaken on the basis of the Hadley Centre climate model chain [*Jones and Reid*, 2001; *Huntingford et al.*, 2003]. In a recent version of this RCM, *Ekström et al.* [2005] found a 10% increase of 1-day precipitation extremes with return periods of 10–50 years across the United Kingdom and more regionally variable changes for 10-day precipitation extremes. Finally, *Semmler and Jacob* [2004] reported, with their RCM, an increase of annual rainfall extremes over most parts of the European continent with particularly large absolute changes over the Baltic Sea area and the central Mediterranean.

[6] In all these published RCM results, there is a common tendency for increases in European precipitation extremes, but there appears to be considerable intermodel variation in the distribution and magnitude of the change. A quantitative comparison of the published results is, however, difficult because of differences in the diagnostics and the techniques with which they were estimated. In principle, intermodel differences in scenarios can arise from the use of different emission scenarios and GCMs and from differences in RCM formulation and technical specifications. The role of these factors for scenarios of mean surface climate is examined by *Déqué et al.* [2005].

[7] The purpose of this study is to compare scenarios of European precipitation extremes for the late 21st century between six different RCMs using consistent diagnostics. The idea is to isolate the contribution to scenario uncertainty, which is due to differences in the formulation of the regional models. Accordingly, all the RCM simulations being analyzed here are based on the same emission scenario (SRES A2 [*Nakicenovic et al.*, 2000]), are nested into the same global climate model (HadAM3H [*Pope et al.*, 2000]), and are operated at comparable grid spacing. Clearly, our analysis satisfies some obvious interest in scenarios of precipitation extremes; however, its results are also relevant for the design of multimodel ensembles, when it comes to estimating the full range of scenario uncertainty. High sensitivity of scenarios to RCM formulation may suggest the consideration of several different RCMs nested in the same GCM, whereas a low sensitivity may suggest that computational resources are used more efficiently in sampling GCM formulation, i.e., by nesting RCMs into several different GCMs.

[8] The diagnostics of primary focus in this analysis are extremes of rainfall with return periods between 5 and 50 years. Their estimation is based on the technique of extreme value statistics [see, e.g., *Coles*, 2001; *Katz et al.*, 2002] very similar to the studies mentioned above. Here this method is applied consistently to all the RCMs and results are compared quantitatively for specific regions. In addition, we also consider more direct diagnostics of average or intense events, which allows us to describe a wider range of the frequency distribution and to employ a simple scaling concept to interpret changes for rare extremes. All our analyses are carried out seasonally stratified in order to identify seasonal variations in scenarios and uncertainties [see also *Wehner*, 2004].

[9] One part of this study is also devoted to an evaluation of the RCMs with respect to their representation of precipitation extremes. Unfortunately, there is currently no comprehensive high-resolution data set that would allow an evaluation for the whole European continent. In this study we consider the European Alps as a test ground. This region has at its disposal a very dense rain gauge network from which an accurate observational data set could be created that is compatible with the grid spacing of the models. Although the Alps cover only a limited part of the model's domain (typically 25 $\times$ 15 grid points), and results may not be extrapolated to other regions, this region is particularly interesting for assessing downscaling abilities because of its complex topography. Also, the evaluation in the Alps complements previous evaluation studies that have focused on more northern parts of Europe [*Booij*, 2002; *Huntingford et al.*, 2003; *Semmler and Jacob*, 2004; *Fowler et al.*, 2005].

[10] The RCM integrations considered in this study were derived as part of a larger multimodel ensemble in the frame of the European project PRUDENCE [*Christensen et al.*, 2006]. The present analysis forms part of an even broader intercomparison of downscaling methods for extremes,

Table 1. Diagnostics of Daily Precipitation Used in This Study

Abbreviation	Definition	Unit
mea	climatological mean precipitation	mm/d
fre	wet day frequency, days with precipitation $\geq$1 mm	fraction
int	wet day intensity, mean precipitation on days with $\geq$1 mm	mm/d
qXX[a]	empirical XX% quantile of precipitation during wet days	mm/d
x1d.TT[b]	return value of 1-day precipitation intensity with a return period of TT	mm/d
x5d.TT[b]	return value of 5-day precipitation intensity with a return period of TT	mm/d

[a]XX = 40%, 60%, 80%, 90%, 95%.
[b]TT = 2, 5, 10, 20, 50, 100 years.

involving statistical and dynamical methods, in the frame of the European project STARDEX [*Goodess*, 2003].

[11] The outline of this paper is as follows. Section 2 describes the statistical procedures used in the analysis of the regional climate models, which are introduced in section 3. Results of the model evaluation in the Alpine region are discussed in section 4. The scenarios of precipitation extremes are presented and interpreted in section 5. Finally, section 6 summarizes the results and draws conclusions.

2. Statistical Analysis

[12] The statistical analysis of this study operates on data sets of 24-hour precipitation totals, simulated by six regional climate models (RCMs) and their parent GCM. Each model was run for a time slice of present climate (1961–1990, also referred to as CTRL) and future climate (2071–2100, SCEN). Details of the experiments and models are described in section 3. For three of the RCMs an ensemble of three integrations is available for both time slices, and these are dealt with simply as a 90-year sample of the corresponding time slice. The ensembles help to reduce estimation errors due to interannual climate variability. All analyses were conducted directly with the data on the native model grids.

[13] We consider a range of different diagnostics with the aim of sampling the frequency distribution of precipitation from moderate to extreme intensities (Table 1). Climatological mean precipitation (mea), wet day frequency (fre), and mean wet day intensity (int) are basic diagnostics of the precipitation occurrence and intensity process. A threshold of 1 mm/d is used to discriminate between wet and dry days. Other choices of the threshold (0.1, 0.5 mm) were found to lead to very similar results. The basic diagnostics will be used primarily for comparison and interpretation of the results for extremes. In addition, several precipitation quantiles (qXX) are considered (Table 1), describing the range from moderate to intense precipitation. Calculated for wet days only, these quantiles describe the precipitation intensity distribution, independently from the wet day frequency. Basic diagnostics and quantiles were calculated using a modified version of the STARDEX diagnostic software tool (user information available at http://www.cru.uea.ac.uk/projects/stardex/deis/Diagnostic_tool.pdf) [*Schmidli and Frei*, 2005].

[14] The diagnostics of primary focus in this study are return values of precipitation intensities with an average recurrence of 5, 10, 20, and 50 years (Table 1). Essentially these are quantiles of the far tail of the frequency distribution. The return value for a return period of T years is defined as the precipitation intensity that is exceeded by an annual or seasonal extreme with a probability of $1/T$. These diagnostics are examined for 1-day (x1d) and 5-day (x5d) precipitation sums, characteristic, respectively, for short-term heavy precipitation, possibly of a convective nature, and extended heavy rainfall periods, related to synoptic disturbances or persistent flow conditions. In Europe, impacts from heavy precipitation are mostly due to short-period rainfalls in summer and multiday episodes in winter, and this is why we focus on the results for 1-day and 5-day extremes in summer and winter respectively.

[15] As in several previous studies concerned with extremes in climate models [e.g., *Zwiers and Kharin*, 1998; *Arora and Boer*, 2001; *Voss et al.*, 2002] we employ the technique of extreme value analysis [see *Fisher and Tippett*, 1928; *Gnedenko*, 1943; *Gumbel*, 1958]. Return values of precipitation extremes are estimated by the block maximum technique, where a generalized extreme value (GEV) distribution is fitted to seasonal precipitation maxima and return values are calculated from that distribution. The GEV is a 3-parameter distribution family with a location, scale and shape parameter. Positive (negative) shapes describe situations where extremes have an upper (lower) bound. (Note that we use the sign convention for shape as given by *Zwiers and Kharin* [1998], which is opposite to that of *Coles* [2001]). The theoretical background and the various techniques of extreme value analysis are explained in detail, for example, by *Coles* [2001] and applications in climatology and hydrology are discussed, for example, by *Palutikof et al.* [1999] and *Katz et al.* [2002]. Our specific application of the block maximum approach is explained in sections 2.1, 2.2, and 2.3.

2.1. Data Selection

[16] Maxima of 1-day and 5-day precipitation intensities are extracted from each season of the 30 (90) years in the two time slices. The analysis is carried out independently for each model grid point and for each season of the year (winter, DJF; spring, MAM; summer, JJA; autumn, SON). For some areas in the Mediterranean region the regional models have simulated extended dry periods in summer, so that precipitation maxima were found to be zero or small in some years. Such "maxima" cannot be considered as being taken from a large sample of data of the precipitation process, which is a theoretical presumption of extreme value analysis. Return values estimated from such samples must be considered unreliable. Therefore an extreme value analysis was only performed for grid points where at least 15 seasonal maxima larger than the intensity of 5 mm/d were simulated in a time slice. Grid points not meeting this criterion are found mostly in southern Europe in summer and particularly in the SCEN integrations, where wet day frequency has substantially decreased. Grid points for which extreme value analysis was not feasible will be masked out in our result plots.

2.2. Estimation

[17] Estimates of the GEV distribution parameters are calculated by the method of maximum likelihood. However, in this study we use a modified form of the classical GEV likelihood function [see, e.g., *Coles*, 2001], which includes a Bayesian prior distribution for the GEV shape parameter.

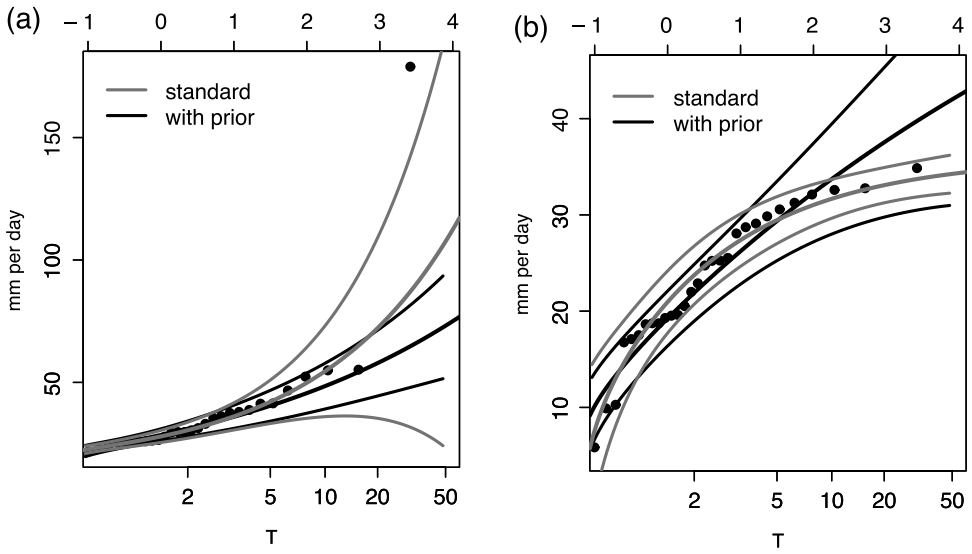

Figure 1. Gumbel diagrams (return value in mm/d as a function of return period T in years) for two grid point samples of daily precipitation extremes, simulated by one of the regional climate models (RCMs) (CHRM, CTRL, winter). The two cases are from nearby grid points in northern France. Sample extremes (dots) and fitted generalized extreme value (GEV) distributions (including pertinent maximum likelihood 95% confidence bands) (solid curves) are depicted. Maximum likelihood estimates of the GEV distribution are displayed for the standard likelihood function (shaded curve) and for the likelihood function with the geophysical prior (solid curve).

This modification was proposed by *Martins and Stedinger* [2000] to prevent the estimation of absurd values of the shape parameter often observed with conventional maximum likelihood estimation from small samples (between 15 to 100 [*Hosking*, 1985; *Martins and Stedinger*, 2000]). Note that alternative robust methods are L moments and regional frequency analysis [*Hosking*, 1985; *Hosking and Wallis*, 1993].

[18] In our application (with sample sizes of 30 or 90), quite many incidents of unrealistic shape estimates were found when using the standard likelihood function. Two selected cases from nearby grid points in northern France are illustrated in Figure 1. In the first case (Figure 1a) the standard method estimates a very heavy tail (shape value is −0.52) because of an outlier value in the sample. In the second case (Figure 1b), the GEV fit levels off and suggests an upper bound near 35 mm/d (shape value is +0.55). Both of these standard estimates appear unrealistic and are not supported by the distributions estimated at adjacent grid points.

[19] The purpose of the geophysical prior distribution is to reduce the likelihood of estimating shape values that are unrealistic in geophysical applications. Figure 2 displays the prior distribution that *Martins and Stedinger* [2000] proposed for hydrological applications and which is used throughout this study. The distribution constrains values of the shape to essentially the range (−0.3, +0.15) and it totally prevents estimates outside (−0.5, +0.5). The prior distribution is biased toward negative shapes. Maximum density is obtained for a shape of −0.1. This is justified for hydrological applications where lower bounds of extremes and hence heavier tails than the Gumbel distribution are very common. Using sample sizes of 25 to 100, *Martins and Stedinger* [2000] show that for GEVs with a negative shape the modified likelihood function leads to much more accurate quantile estimates (in terms of root mean square error) compared to the standard likelihood, the moment, and the L moment [*Hosking*, 1990, 1992] estimators. Moreover, in many cases the bias is smaller or at least comparable to that of other estimators.

[20] In Figure 1, GEV distributions estimated from the modified likelihood function are also depicted. The resulting distributions seem physically more meaningful (shape parameters are −0.27 for case a and 0.12 for case b). The modification influences, in particular, quantiles at return periods of 10 years and more. The stabilizing effect of the

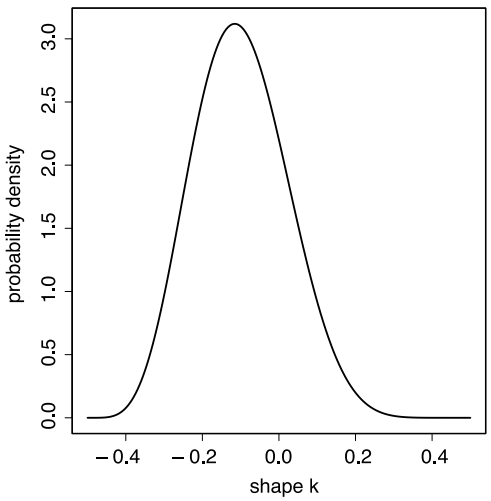

Figure 2. Probability density of the prior distribution for the GEV shape parameter. The prior distribution is used in this study to improve the robustness of maximum likelihood estimates of GEV parameters and quantiles. Adapted from *Martins and Stedinger* [2000].

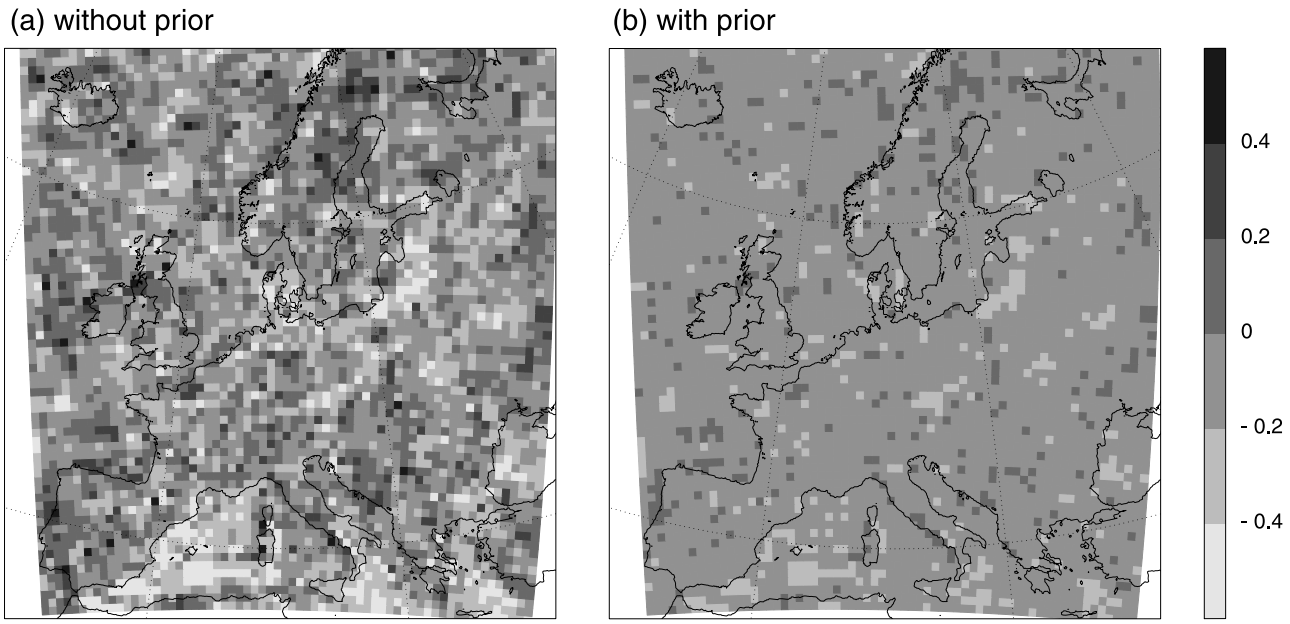

Figure 3. Distribution of the GEV shape parameter estimated from grid point extremes (a) without and (b) with geophysical prior. Results are from a 30-year time slice of one of the RCMs (CHRM, CTRL).

geophysical prior is also demonstrated in Figure 3, showing the spatial distribution of the shape parameter for one of the models' control integrations. When estimated with the standard likelihood function (Figure 3a), the shape shows an irregular pattern, with many anomalous values even over the ocean. More than 5% of the grid points exhibit shape values outside the range (−0.4, +0.4) in this example. In contrast, estimates with the modified likelihood function (Figure 3b) are much less variable and smoother in distribution. Note also, that in case of the standard estimation, negative shape values were estimated for more than 70% of the grid points and that the median across Europe is −0.09. This is close to the density maximum of the prior distribution and it justifies the choice of a prior distribution that is shifted to negative values.

2.3. Confidence Intervals and Statistical Tests

[21] In this study we use two different methods for the assessment of uncertainties. On a grid point basis, likelihood confidence intervals for return values were calculated directly from the observed information matrix of the modified likelihood function [see, e.g., *Coles*, 2001, section 3.3.3]. A confidence interval for the difference in return values between the CTRL and SCEN sample is then derived from the standard errors in each sample, assuming normal distribution of errors. This provides a statistical test for the change. Note that the asymptotic properties of likelihood confidence intervals (symmetry and normal errors) may not be satisfied with the small samples considered. We therefore view the results only as an approximate indication. Likelihood confidence is used for mapping the statistical significance in maps of the change later in section 5.

[22] A more accurate, bootstrap based, estimation of confidence intervals is used for spatial averages of return values across selected subdomains. The subdomains used are depicted in Figure 4. Bootstrap samples of domain mean return values were generated by resampling of years (nonparametric bootstrap). In order to preserve the spatial correlation of errors, all grid points within the subdomain are sampled from the same years [see, e.g., *Wilks*, 1997]. GEVs are then estimated for each grid point sample and return values averaged over the subdomain. 50 bootstrap samples were generated for each time slice. Confidence intervals for the relative change in return values between CTRL and SCEN are then obtained by resampling between the pairs of bootstrap samples.

3. Models and Experiment

[23] The RCM integrations analyzed in this study were conducted by nesting into the atmosphere-only GCM (HADAM3H) of the Hadley Centre at the U.K. Met Office. One RCM is also nested into HADAM3P, a more recent version of the same GCM (see later). HADAM3H was derived from the coupled atmosphere-ocean model HadCM3 [*Gordon et al.*, 2000; *Johns et al.*, 2003] and is described by *Pope et al.* [2000]. The HADAM3H integrations, from which the forcing fields for the RCMs were taken, have a resolution of about 150 km in midlatitudes and they extend over the two time slices 1961–1990 (CTRL) and 2071–2100 (SCEN). For CTRL, HADAM3H was forced by observed sea surface conditions of the same period by prescribing the evolution of sea surface temperature and sea ice distribution. For SCEN, sea surface conditions were constructed from observations and anomalies from a transient integration of HADCM3 using the IPCC SRES A2 emission scenario [*Nakicenovic et al.*, 2000]. With this scenario HADAM3H has simulated a global mean surface temperature increase of 3.18 K between CTRL and SCEN (D. Rowell, personal communication, 2004). This is in the upper half of the warming range predicted by the IPCC [*Cubasch et al.*, 2001] and corresponds approximately to the 55%

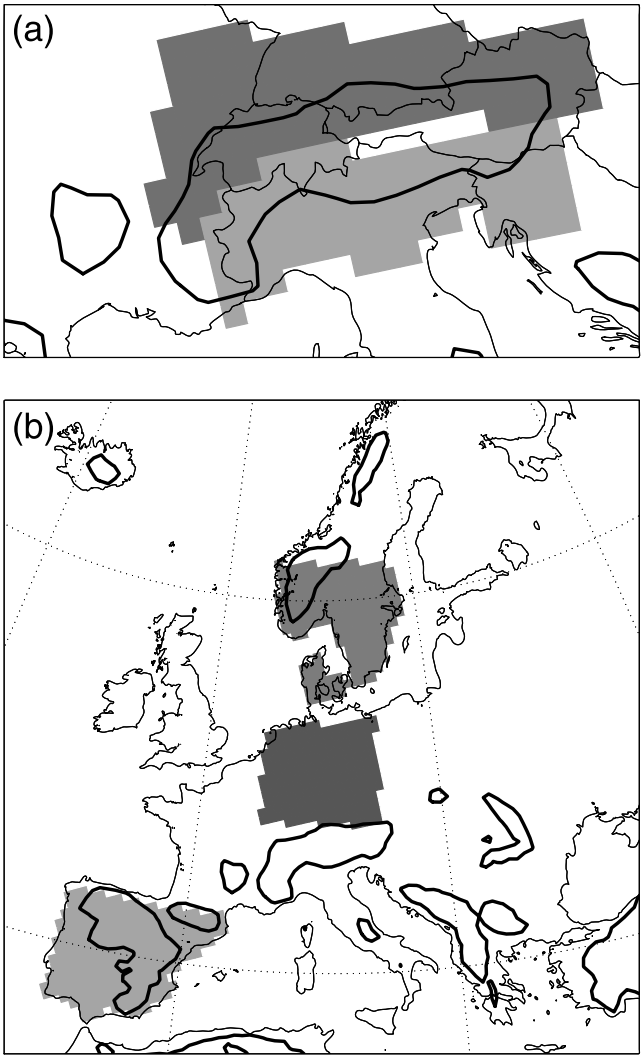

Figure 4. Subdomains used in the analysis of this study: (a) Northern and southern Alps and (b) southern Scandinavia, central Europe, and Iberia. Subdomains vary slightly between models because of different grids and land-sea masks. Figure 4 is for model SMHI.

quantile of the probabilistic prediction of *Wigley and Raper* [2001] for the warming between 1990 and 2100.

[24] Three integrations were carried out with HADAM3H (and also with HADAM3P) for both time slices, starting from different initial conditions. Two of the considered RCMs were integrated from all six members. The remaining four RCMs ran for only one (but the same) pair of ensemble members. Consideration of ensemble integrations is particularly valuable in the analysis of extremes, because quantiles can be estimated from a larger sample and uncertainty arising from interannual variations is reduced.

[25] The RCMs considered in this study are operated at a grid spacing of about 50 km, with a comparable domain, covering the European continent from the Mediterranean to Scandinavia and from Iceland to the Black Sea. Domains for some of the models are depicted by *Frei et al.* [2003]. All six RCMs are state-of-the-art limited-area climate models with one-way nesting over a lateral boundary zone. The boundary zone is excluded from all analyses and displays in this paper. Table 2 gives a list of the RCMs with acronyms, basic characteristics and references to more technical descriptions. It may be of interest to mention that there are relationships between some of the models. CHRM and REMO share the same dynamical core. CHRM and GKSS have very similar physical parameterizations. The same is the case for HIRHAM and REMO.

[26] For the regional model of the Hadley Centre, two model versions (HADRM3H and HADRM3P) will be considered in our analysis. The more recent model (HADRM3P) uses a newer version of physical parameterizations (mainly with effects on the vertical cloud profile (R. G. Jones et al., A high resolution atmospheric GCM for the generation of regional climate scenarios, manuscript in preparation, 2005)). However, the boundary conditions for the newer model are taken from the corresponding new version of the atmospheric GCM (HADAM3P), and hence the integration with HADRM3P is not strictly in our common setting. Results of HADRM3P will therefore not be displayed as extensively as for the other models, but eventual comparison to its predecessor HADRM3H is interesting, primarily because it is the new version, which is used in many current impact studies.

[27] The RCM experiments used in this study form part of an even larger collection of downscaling experiments, conducted in the EU project PRUDENCE [*Christensen et al.*, 2006]. The large effort required with the handling of daily data sets, with extreme value analysis and resampling experiments has prevented us from considering all available experiments. A comparison of scenarios for mean seasonal surface climate with all PRUDENCE RCMs was, however, given by *Déqué et al.* [2005].

4. Evaluation in the Alpine Region

[28] This section presents an evaluation of the climate of precipitation extremes as simulated by the CTRL integrations of the RCMs. Results are discussed/depicted only for a selection of the diagnostics considered in this study (Table 1), but the selection provides a representative picture of the models' behavior. The evaluation is conducted for the European Alps, a 1100 $\times$ 700 km^2 region, encompassing typically 25 $\times$ 15 model grid points. The Alps are located well in the interior of all the model domains, usually slightly south of the domain centers. This high mountain area is an ambitious but interesting test ground as it illustrates the downscaling ability of RCMs. Our focus on the Alps is because we dispose of a high-density precipitation data set for this region, which provides a suitable observation reference. Unfortunately no similar data set is currently available for Europe as a whole and it is difficult to extrapolate the results of this evaluation to other regions. Also, it should be born in mind that discrepancies of the RCMs to the observations may also be due to errors in the driving GCM, and need not necessarily point to errors in the RCMs themselves.

4.1. Evaluation Data Set

[29] The observational reference for the present study is very similar to that used in a previous evaluation of reanalysis-driven RCMs by *Frei et al.* [2003]. In summary

Table 2. Regional Climate Models From Which Integrations Are Analyzed in This Study

Model Acronym	Institution/Model Origin and Relevant References[a]	$nx \times ny$	Δx	Levels	Global Climate Model	Number of Ensemble Members,CTRL/SCEN[b]
CHRM	Swiss Federal Institute of Technology (ETH), Zürich, Climate High-resolution Model. Climate version of "Europamodell" of German and Swiss weather services. Model: *Lüthi et al.* [1996]; *Vidale et al.* [2003] Temperature Extremes: *Schär et al.* [2004]	81 × 91	0.5°	20	HADAM3H	1/1
GKSS	GKSS, Institute for Coastal Research, Geesthacht, Germany Climate Version of "Lokalmodell'' of German Weather Service Model: *Steppeler et al.* [2003] Wind extremes: B. Röckel and K. Woth (Future changes in near surface wind extremes over Europe from an ensemble of RCM simulations, submitted to *Climate Change*, 2005); *Woth et al.* [2005]	101 × 107	0.5°	20	HADAM3H	1/1
HADRM3H	Hadley Centre, U.K. Meteorological Office, Exeter Regional model of climate model suite at the Hadley Centre. Model: *Jones et al.* [1995, 1997]; see also *Pope et al.* [2000]. Prec. Extremes: *Huntingford et al.* [2003]; *Fowler et al.* [2005]; *Ekström et al.* [2005]	106 × 111	0.44°	19	HADAM3H	3/3
HADRM3P	Hadley Centre, U.K. Meteorological Office, Exeter Regional model of climate model suite at the Hadley Centre. Updated version of HADRM3H Model: *Jones et al.* [2004]	106 × 111	0.44°	19	HADAM3P	3/3
HIRHAM	Danish Meteorological Institute, Copenhagen Dynamical core from HIRLAM, Parameterizations from ECHAM4 Model: *Christensen et al.* [1996]; *Roeckner et al.* [1996] Physiographic data: *Hagemann et al.* [1999] Prec. extremes: *Christensen and Christensen* [2003, 2004]	110 × 104	0.44°	19	HADAM3H	3/3
REMO	Max Planck Institute for Meteorology, Hamburg, Germany Dynamical core from Europamodell of German Weather Service. Parameterizations from ECHAM4. Model: *Jacob* [2001]; *Roeckner et al.* [1996] Prec. extremes: *Semmler and Jacob* [2004]	97 × 109	0.5°	20	HADAM3H	1/1
SMHI	Swedish Meteorological Institute, Stockholm Rossby Centre Atmosphere Ocean Model Model: *Jones* [2001]; *Meier et al.* [1999] Surface climate change: *Räisänen et al.* [2004]	106 × 102	0.44°	24	HADAM3H	1/1

[a]Given here are technical descriptions and other recent analyses of climate change experiments with the models.
[b]CTRL indicates a time slice of present climate (1961–1990), and SCEN indicates future climate (2071–2100).

it is a gridded precipitation analysis for every day of the 20 years 1971–1990 based on data from the operational high-resolution rain gauge networks encompassing more than 6500 station records. The analysis grid has a resolution comparable to the grid spacing of the RCMs, and the analysis scheme estimates averages of the rainfall intensity over grid pixels, ensuring compatibility of the resulting statistics with the resolution of the models [see, e.g., *Osborn and Hulme*, 1997; *Frei et al.*, 2003]. At each grid point, 10–50 station values contribute to the analysis. Deviating from the work by *Frei et al.* [2003], the analysis for this study was performed with a climatological scaling similar to that used by *Widmann and Bretherton* [2000]. This procedure uses a gridded high-resolution climatology, in our case that of *Schwarb et al.* [2001], to derive relative anomalies of observed daily precipitation totals. The relative anomalies are gridded, in our case using a variant of the Shepard algorithm [*Shepard*, 1984; see also *Frei and Schär*, 1998], and, finally, the fields of relative anomalies are augmented with the same climatology. The climatological scaling reduces errors of the analysis emanating from biases in station distribution, e.g., the underrepresentation of high-elevation areas, because such biases are explicitly considered in the derivation of the climatology.

[30] It should be noted that our gridded analysis is affected by systematic undercatch of the underlying rain gauge measurements [*Neff*, 1977; *Groisman and Legates*, 1994]. In the Alpine region this error ranges from 4% at low elevations in summer to more than 40% above 1500 m above sea level in winter [*Sevruk*, 1985]. In the average over larger-scale subdomains, such as those in Figure 4a, we estimate that the gridded analysis underestimates mean precipitation by about 11% in winter and 6% in summer [see *Frei et al.*, 2003, Table 1].

[31] The diagnostics of Table 1 for observations were determined from the daily gridded analysis in the same way as for the models. Unfortunately, it was not possible to cover a 30-year period with our analysis as in the models, because of limited data availability in the 1960s and problems in data quality in the 1990s. More details about the data set and analysis technique are given by *Frei and Schär* [1998] and *Frei et al.* [2003].

4.2. Results

[32] In the Alps the highest frequency of heavy precipitation occurs in autumn. It is therefore natural to have a special focus on this season first. Figure 5 compares the distribution of the 5-year return value of 1-day precipitation extremes (x1d.5, see Table 1) between observations (Figure 5, top right) and models. In autumn, heavy precipitation is frequently associated with moist and weakly stratified airflows from the south, often with embedded convection. Accordingly, large values of x1d.5 are observed along the southern rim of the Alps, with a characteristic mesoscale pattern (note areas exceeding 80 mm/d), reflecting topographic detail of the ridge and the proximity of the Mediterranean Sea. All RCMs reproduce the general southern rim pattern quite well and several models show features similar to the observed peaks, although eventually shifted by a few grid points (e.g., the Massif Central maximum in CHRM and GKSS). HADRM3H and HADRM3P show very similar distributions. Both tend to overestimate the topographic enhancement at the southern rim but underestimate the return values in the foreland (the Po valley). HIRHAM and SMHI show an overall underestimate and GKSS tends to overestimate return values.

[33] Comparison of the RCM results to those of their driving GCM (HADAM3H (Figure 5, top left)) reveals the benefit from the higher model resolution. Although the GCM reflects the larger-scale pattern of the observations reasonably well, the RCMs depict much more realistic structures in connection with the finer-scale features of the topography. Note that the mesoscale pattern in x1d.5 is not trivial (e.g., a simple height dependence) and hence this evaluation illustrates the downscaling ability of RCMs for precipitation extremes.

[34] It is interesting to note that despite the rareness of events considered, the correspondence of the RCM simulated x1d.5 pattern with observations is only slightly lower than that found in a previous evaluation for the 90% quantile (event recurrence one month) and for reanalysis-driven RCMs [*Frei et al.*, 2003]. Indirectly, this attests to the quality of the GCM (HadAM3H and HadAM3P) in reproducing, at least in this season, the observed climate of large-scale flow conditions relevant for precipitation extremes in the Alps.

[35] In a visual comparison of x1d.5 for winter and spring (not shown) we found a similar skill of the RCMs to that found in autumn, but the biases and intermodel differences were largest in summer. Figure 6 shows the seasonal variation in some of the precipitation diagnostics averaged over 2 Alpine subdomains and Table 3 lists numbers of the model biases for winter and summer (domain definitions are displayed in Figure 4a). For x1d.5 (Figures 6e and 6f) the observed interseason and across-ridge variations are reasonably reproduced by individual models although there are, in cases, substantial biases. An exception to this is summer in the southern Alpine region, where in contrast to observations all models, except GKSS, simulate smaller values of x1d.5 than in winter and spring. A similar dry bias was found for mean precipitation in the southern Alps [see also *Frei et al.*, 2003], and it is likely related to problems in the representation of the summertime water and energy cycle in southern Europe [e.g., *Noguer et al.*, 1998; *Hagemann et al.*, 2004; *Hirschi et al.*, 2006]. In the other seasons, however, the biases are more model specific. Both HADRM3 models and the GKSS tend to overestimate and CHRM, HIRHAM, SMHI, and REMO tend to underestimate x1d.5. Note that even though the uncertainty in x1d.5 from interannual variations is quite large, most of the model biases well exceed the 90% confidence ranges, implying that the depicted model biases are not artifacts of random errors due to the short observation/simulation periods.

[36] Interestingly, the model biases for the tail of the distribution (x1d.5) are, in relative terms, comparable to or smaller than the biases in either wet day intensity or mean precipitation (Table 3). At least we do not find indications of systematically larger biases for quantiles of extremes up to a recurrence of five years compared to more average precipitation statistics. It is also worth noting that the intermodel pattern and seasonal variation of biases is very similar between int and x1d.5 (Figures 6c–6f), suggesting that the model errors in precipitation extremes are primarily related to deficiencies in the intensity process rather than the

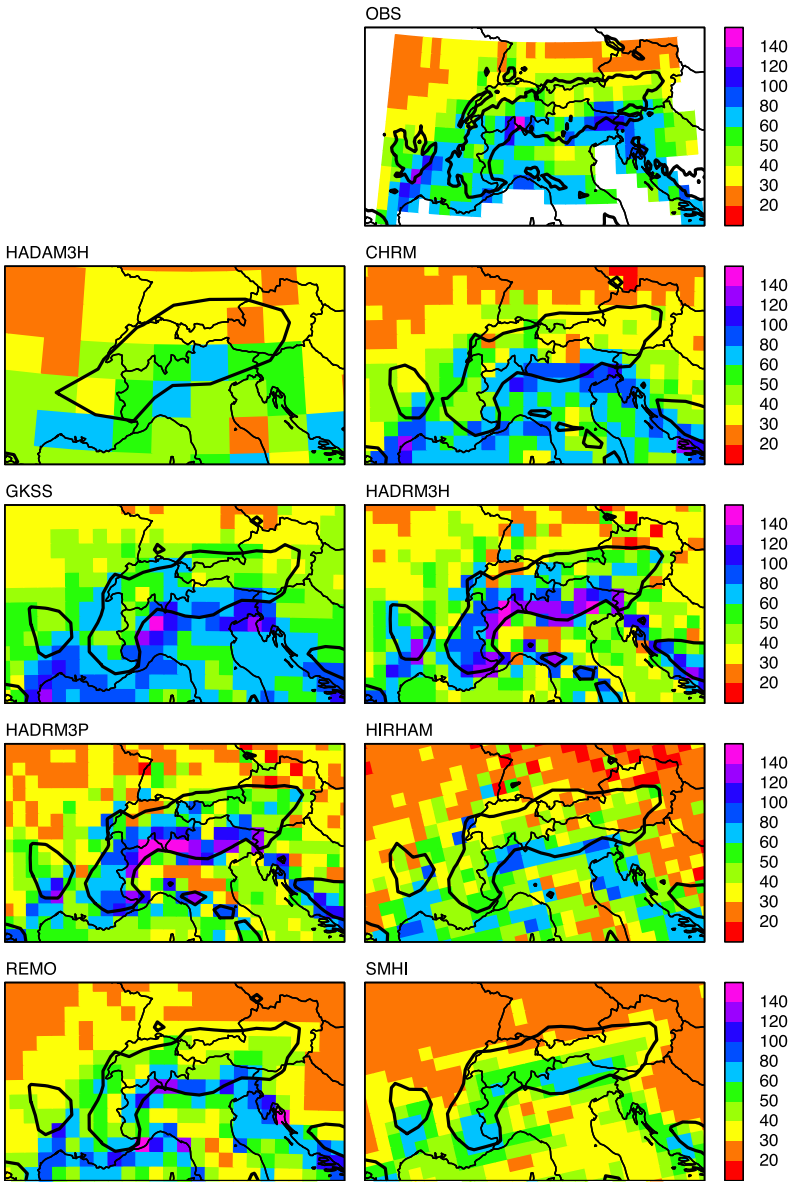

Figure 5. Five-year return value of 1-day precipitation extreme (x1d.5, mm/d) in autumn (September–November). Shown are observations (OBS, 1971–1990, top right), the common general circulation model (GCM) (HADAM3H, 1961–1990, top left), and RCMs (1961–1990). Model results are shown on original model grids. Thick lines are 700 m above sea level contours of pertinent model topography. Topography in OBS is more detailed.

occurrence process. Indeed, the bias pattern and seasonal variation of the wet day frequency (fre, Figures 6a and 6b) is quite different from int and x1d.5. All models overestimate wet day frequency in the northern Alps from autumn to spring. This is likely due to errors in the driving GCM, because no similar bias was seen in reanalysis-driven integrations with the same RCMs [see *Frei et al.*, 2003].

[37] In summary, the present evaluation demonstrates that RCMs are capable of reproducing nontrivial mesoscale patterns of observed precipitation extremes in the Alps, at least during dynamically active seasons. Nevertheless, there are model specific biases of up to several tens of percent, especially in summer; however, the model performance for rare extremes is not worse than for less extreme quantiles or for mean wet day intensity. The evaluation did not reveal previously undiscovered model deficiencies that are specific to rare extremes. Instead, we expect that future improvements in the modeling of the precipitation intensity process will also significantly reduce current biases for rare extremes.

[38] It is unclear to what extent the results in the Alps are representative for other European regions, but published evaluations suggest biases of a similar magnitude in some regions of central and northern Europe, such as the British Isles [*Huntingford et al.*, 2003; *Fowler et al.*, 2005], the Meuse catchment in western Europe [*Booij*, 2002] and southern Germany [*Semmler and Jacob*, 2004]. No evaluations of heavy precipitation statistics are so far available for

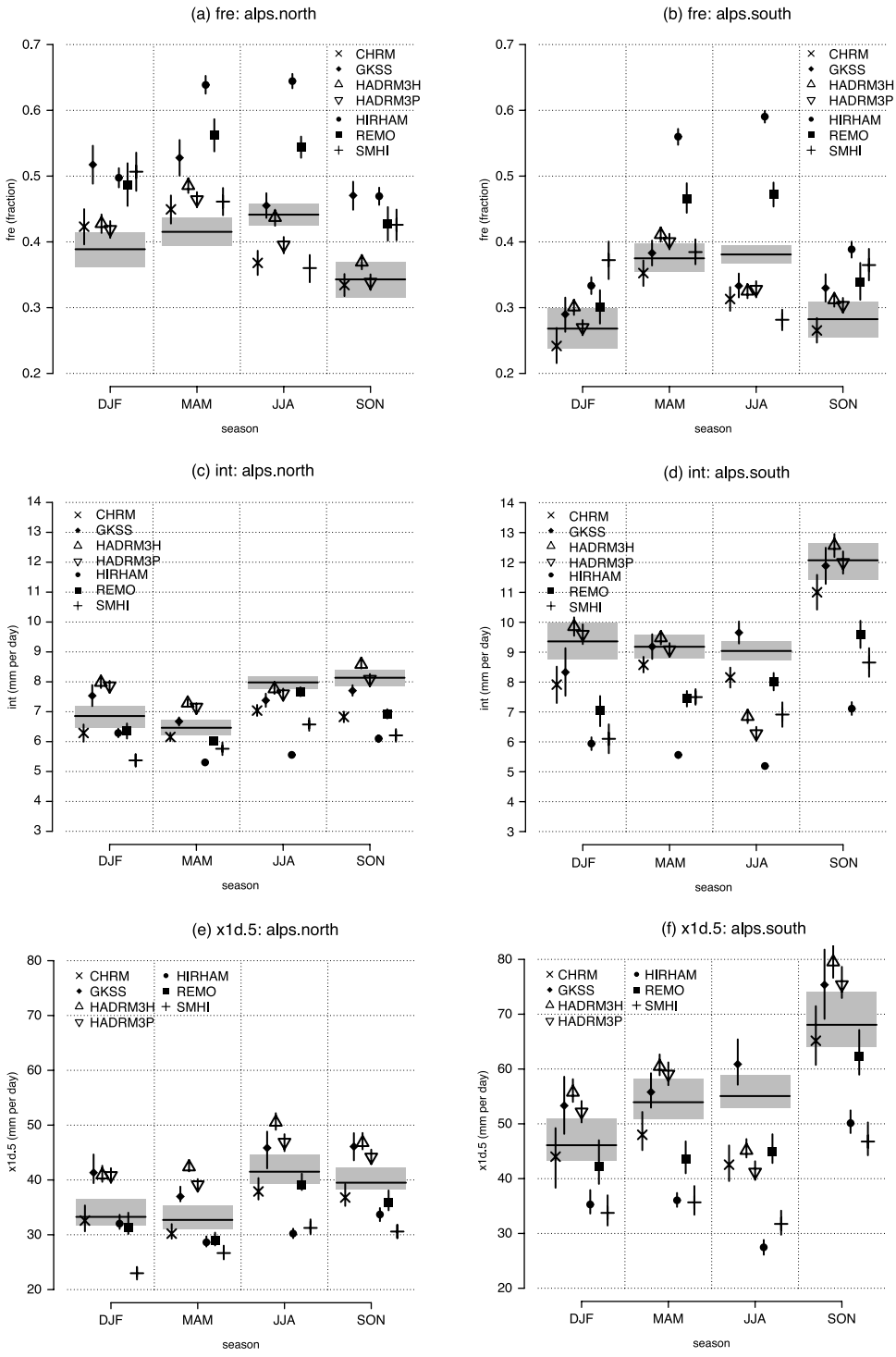

Figure 6. Best estimate and 90% bootstrap confidence interval of (a and b) wet day frequency (fre, fraction), (c and d) wet day intensity (int, mm/d), and (e and f) the 5-year return value of 1-day precipitation (x1d.5, mm/d) for RCMs (symbols and vertical lines) and observations (horizontal lines, shaded area). Results are shown for two subdomains (northern Alps, Figures 6a, 6c, and 6e, and southern Alps, Figures 6b, 6d, and 6f; see Figure 4).

regions of southern Europe. However, for mean precipitation most of the regional models considered in this study were shown to be too dry in southern and southeastern Europe, in particular in summer [e.g., *Noguer et al.*, 1998; *Hagemann et al.*, 2001; *Vidale et al.*, 2003; *Räisänen et al.*, 2004; *Hirschi et al.*, 2006]. The dryness is particularly pronounced in summer, and it goes along with model biases in soil moisture and components of the surface water and energy budgets [see also *Hagemann et al.*, 2004]. These results may indicate that the results of this study for

Table 3. Bias of RCM Control Simulations in Domain Mean Precipitation Diagnostics for the Northern and Southern Alps[a]

	December–February				June–August			
	fre, %	mea, %	int, %	x1d.5, %	fre, %	mea, %	int, %	x1d.5, %
Northern Alps								
CHRM	+9	+1	−8	−2	−17	−26	−12	−9
GKSS	+33	+46	+10	+24	+3	−5	−8	+10
HADRM3H	+10	+36	+16	+23	−1	+1	−3	+22
HADRM3P	+8	+32	+15	+23	−10	−10	−5	+13
HIRHAM	+28	+19	−8	−4	+46	+3	−30	−27
REMO	+25	+16	−7	−6	+23	+20	−4	−6
SMHI	+30	+3	−22	−31	−18	−29	−18	−25
Southern Alps								
CHRM	−10	−23	−15	−5	−18	−25	−10	−23
GKSS	+8	0	−11	+16	−13	−10	+7	+11
HADRM3H	+12	+26	+5	+21	−15	−25	−24	−18
HADRM3P	+1	+10	+3	+13	−14	−30	−31	−25
HIRHAM	+24	−18	−37	−23	+55	−10	−43	−50
REMO	+12	−17	−25	−8	+24	+15	−11	−19
SMHI	+39	−1	−35	−27	−26	−31	−24	−42

[a]See Table 1 and Figure 4a. Numbers are in percent of observations.

southern Europe in summer should be considered with more reservation.

5. Simulated Change in Precipitation Extremes

[39] This section describes the distribution and magnitude of the change in precipitation extremes between the CTRL and SCEN time slices as simulated by the six RCMs and the GCM. We discuss the coherence/variation of the change between the models, and examine how the change in extreme events is related to the change in average events. This will help us to understand the nature of the differences between the models. Detailed discussions will be presented in the first two subsections for winter and summer, the two seasons for which fundamentally different intermodel variations were found. A brief discussion of the results for the transition seasons is then provided in the last subsection.

5.1. Winter

[40] Figure 7 depicts the change in the 5-year return value of 5-day precipitation intensity in winter (x5d.5, DJF, see Table 1). Here the 5-day intensity was chosen because adverse impacts in winter are mostly due to multiday heavy precipitation, but in fact, the result for extreme 1-day events (x1d.5, not shown) is very similar. Maps are displayed for the driving GCM (HADAM3H, top right panel) and those 6 RCMs that were nested into HADAM3H. The result for HADRM3P, which was nested in a more recent version of the GCM (see section 3), is very similar to that of HADRM3H.

[41] The continental-scale pattern of the change shows an increase over large areas north of about 45°N and small changes or a decrease south of 45°N. Small changes of variable signs are also noted over the high latitudes of the northeastern Atlantic. For large areas of central and northern Europe, the increase is statistically significant (at the 5% level) even at the scale of single model grid points. The larger-scale pattern is very similar between the regional models. This is also true when comparing models with three ensemble members (HADRM3H, HIRHAM) with those consisting of one member only. The longer simulation period of the former primarily results in larger areas with statistically significant changes but does not affect the overall pattern. Note that the larger-scale pattern simulated by the RCMs closely resembles the result for the GCM, but RCMs exhibit more detail especially along the costs and in the Alps.

[42] A quantitative comparison is provided in Table 4, where the relative change in the domain mean return value x5d.5 is listed for the three European subdomains (see Figure 4a) and for all models (including HADRM3P). The sign of the change is consistent among the models in southern Scandinavia, with increases of 10–25%, and in Iberia with decreases of 7–14%. In southern Scandinavia, the increase is statistically significant (based on the 95% resampling confidence interval; see section 2.3) for all models. In central Europe the model results vary in sign, which is also obvious from Figure 7. Here the models with one ensemble member exhibit consistently smaller increases, even a slight decrease in the case of CHRM and HADAM3H (the GCM), compared to the three-member models (HADRM3H, HADRM3P, and HIRHAM). (Note that for the GCM we had precipitation data only from one ensemble member.) Indeed, interannual variations mostly explain the intermodel variations in this region: The integrations of HADRM3H and HIRHAM for the particular ensemble member common to all the other models, exhibit a change of x5d.5 by 0% and +1% respectively in central Europe, which is very similar to the results from the other models. It appears that the common pair of ensemble members had an anomalously small response in central Europe and we could expect a fairly consistent increase in the order of about 10% if all RCMs had integrated all ensemble members.

[43] What does the change in return values mean in terms of changes in the recurrence of precipitation extremes? This is addressed in Figure 8, which compares return periods for equal domain mean return values between the CTRL (horizontal axis) and SCEN (vertical axis) time slices. The comparison reveals that the future 5-year return value in southern Scandinavia corresponds to extremes with a return period of 8–18 years under present-day conditions, depending on the model. Similarly, the 20-year return value of future climate corresponds to events with a recurrence of 40–100 years under present climate. Hence for very rare precipitation extremes the models simulate a frequency increase by a factor of 2 to 5 over northern Europe in winter. The corresponding numbers for central Europe are from no change to a frequency increase by a factor of about 2.

[44] It is instructive to compare the change for rare extremes, obtained by means of extreme value analysis, to that for average or intense events as revealed by more basic diagnostics of the precipitation frequency distribution. Such a comparison is displayed in Figure 9 for all three European subdomains. In each panel the three columns to the left (fre, mea, and int) describe basic properties of the precipitation occurrence and intensity process and the remaining columns (q40, . . ., x5d.50) provide a section across the distribution from moderate to extreme precipitation events. Note that there is a subtle difference in that qXX are quantiles of the

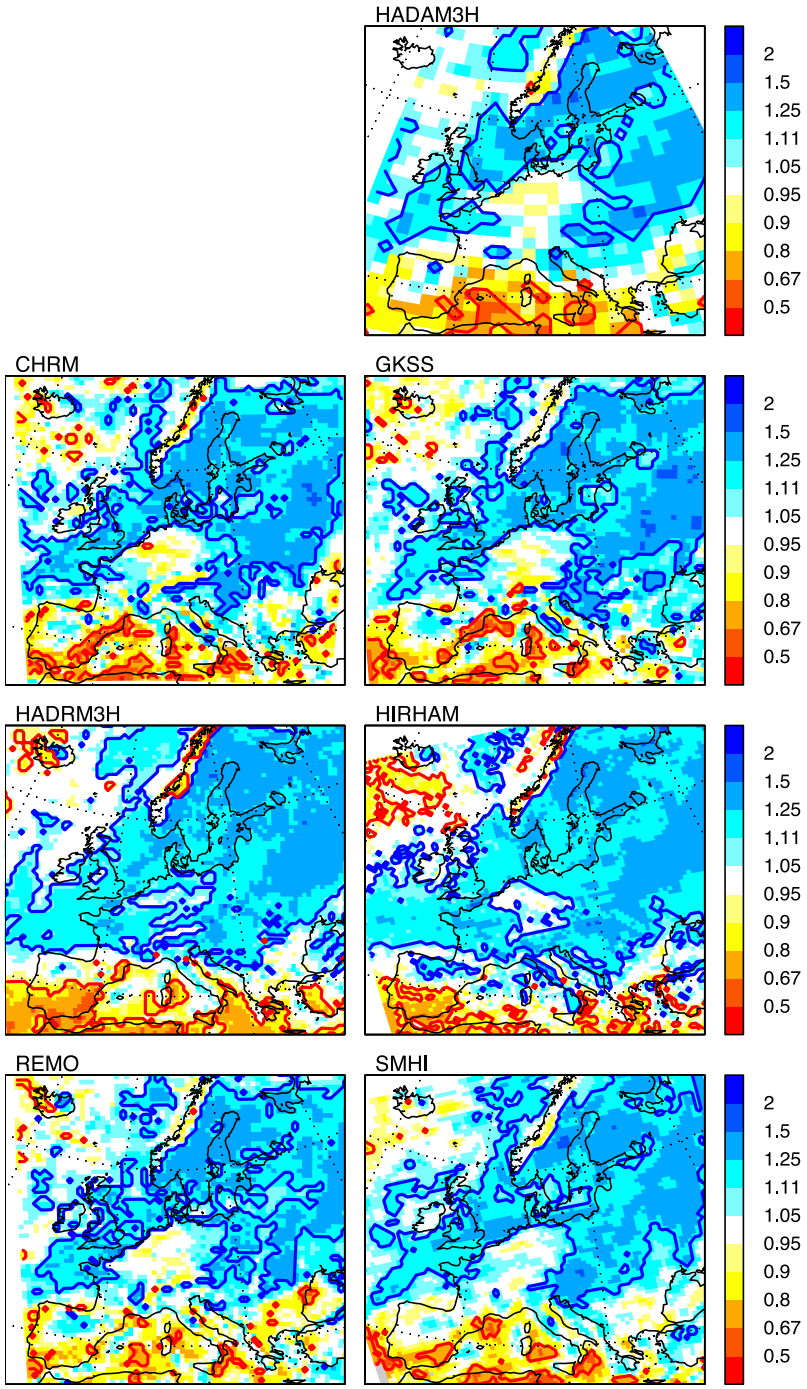

Figure 7. Ratio (SCEN (2071–2100)/CTRL (1961–1990)) of the 5-year return value for 5-day precipitation intensity (x5d.5) in winter (December–February). Results are given for the driving GCM (top right) and for six RCMs under the A2 emission scenario (see Table 2). Note the log scale in color coding. Blue (red) curves indicate areas with a statistically significant (5%) increase (decrease) in an independent test at each model grid point (maximum likelihood confidence; see section 2.3).

sample of wet days, while x5d.T are return levels for the sample of wet and dry days together (Table 1).

[45] Figure 9 reveals that the structure of the change across the precipitation distribution is very coherent between the models in winter. For example, in southern Scandinavia and central Europe, there is an approximately equal relative increase in wet day frequency and intensity, which is mostly statistically significant and is reflected in an increase of mean winter precipitation. Moreover, the change in wet day quantiles (q40 and q90) is very similar to the change in wet day intensity. Also, the change for extreme quantiles (x5d.T), although different between models, varies very little between return periods and is similar in magnitude to the change in wet day intensity of the corresponding

Table 4. Change (Ratio SCEN/CTRL) in the 5-Year Return Value of 1-Day (5-Day in DJF) Precipitation Intensity for Subdomains of Figure 4a[a]

	DJF, x5d.5	MAM, x1d.5	JJA, x1d.5	SON, x1d.5
		Southern Scandinavia		
HADAM3H	**1.21**	**1.22**	1.06	1.09
CHRM	**1.22**	**1.27**	**1.18**	**1.15**
GKSS	**1.25**	**1.19**	**1.21**	**1.15**
HADRM3H	**1.17**	**1.18**	1.03	**1.11**
HADRM3P	**1.10**	**1.16**	1.02	**1.10**
HIRHAM	**1.15**	**1.18**	**1.18**	**1.15**
REMO	**1.21**	**1.18**	**1.34**	**1.23**
SMHI	**1.16**	**1.19**	1.05	**1.15**
		Central Europe		
HADAM3H	0.98	**1.17**	1.07	**1.11**
CHRM	0.98	**1.12**	**1.21**	**1.22**
GKSS	1.00	**1.12**	**1.12**	**1.15**
HADRM3H	**1.10**	**1.14**	0.95	**1.11**
HADRM3P	**1.11**	**1.16**	**0.87**	**1.09**
HIRHAM	1.07	**1.16**	**1.09**	1.06
REMO	1.00	**1.24**	**1.19**	**1.21**
SMHI	1.05	**1.23**	**1.13**	**1.18**
		Iberia		
HADAM3H	0.93	**0.87**	–	0.95
CHRM	0.86	**0.86**	–	0.99
GKSS	0.90	**0.89**	–	1.00
HADRM3H	**0.86**	**0.88**	–	0.99
HADRM3P	**0.88**	**0.86**	–	0.95
HIRHAM	0.93	0.94	–	0.96
REMO	0.92	**0.87**	–	0.99
SMHI	0.91	**0.91**	–	1.02

[a]Shown are the results for the GCM (HADAM3H, from one ensemble member only) and seven RCMs. Bold numbers indicate changes that are statistically significant; that is, the ratio of 1.0 (no change) is outside the 95% confidence interval obtained by resampling (see section 2.3). Results for Iberia in summer are omitted because extreme value analysis was not feasible for many grid points with the small number of rainy days. DJF, December–February; MAM, March–May; JJA, June–August; SON, September–November.

model. Exceptions to this are CHRM, GKSS, and REMO in central Europe, which show a slight decrease in extreme quantiles contrasting with the increase in wet day intensity.

[46] The general picture arising from this is that the precipitation frequency distribution in winter has changed essentially like a simple rescaling, where the relative change in quantiles is independent of frequency and the change for wet day intensity is a reasonable estimate of the change in extreme return values. This result conforms to expectations from a simple scaling model where frequency and intensity changes are equally distributed across the frequency distribution. *Fowler and Hennessy* [1995] illustrated that the changes in extremes resulting from such a scaling are dominated by the effect of intensity changes over those by frequency changes. In Appendix A we provide a similar illustration for quantiles. A quantitative assessment of the changes in return values using the scaling model is presented further below.

[47] For subdomain Iberia, the situation is somewhat more complex (Figure 9, bottom). Extreme return values decrease more than the wet day intensity. However, a clear interpretation of the changes for this region is difficult because of the large estimation uncertainty. In Iberia, the change in any of the basic diagnostics (fre, mea, int, qXX) is statistically not significant for all models, and only two models (HADRM3H and HADRM3P) show a significant decrease for extreme return values (see Table 4).

[48] Let us examine to what extent the simulated change in extreme return levels can be quantitatively explained by a simple rescaling of the precipitation frequency distribution. For this purpose we derive, for each model, a hypothetical distribution function for the SCEN period by scaling the corresponding CTRL distribution. The scaling consists of the following steps: The distribution of return levels under CTRL is transformed into a conditional distribution for wet days only, using the simulated wet day frequency of CTRL. The resulting distribution is scaled (multiplying quantiles) using the simulated relative change in wet day intensity, and the result is considered as a conditional distribution (i.e., for wet days only) under SCEN. Finally an unconditional distribution for SCEN is determined using the simulated wet day frequency for SCEN. This procedure is formalized in

$$X'_{SCEN}(T) = \frac{i_{SCEN}}{i_{CTRL}} \cdot X_{CTRL}\left(\frac{f_{SCEN}}{f_{CTRL}} \cdot T\right). \quad (1)$$

where $X'_{\mathrm{SCEN}}(T)$ is the scaled quantile function for SCEN, X_{CTRL} is the simulated quantile function under CTRL, $f_{\mathrm{SCEN}}/f_{\mathrm{CTRL}}$ is the ratio of simulated wet day frequencies and $i_{\mathrm{SCEN}}/i_{\mathrm{CTRL}}$ the ratio of simulated wet day intensities. Hence the scaling exercise estimates future return levels purely from the simulated changes in wet day frequency and intensity, assuming that these changes are independent of event intensity. A similar scaling and its effect on

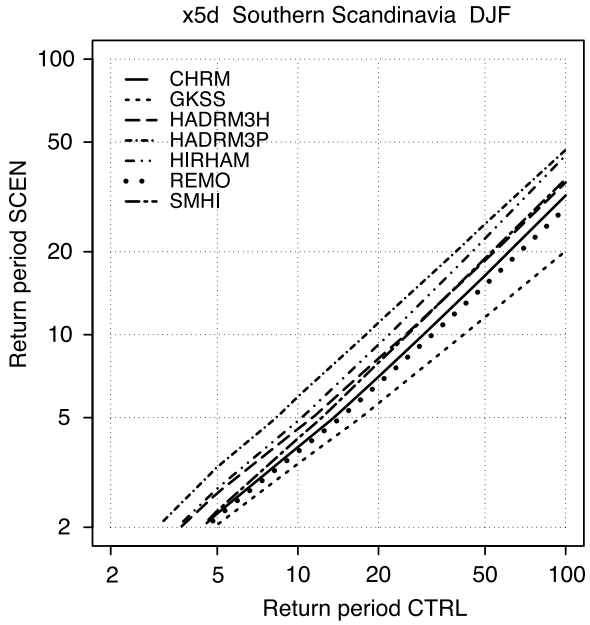

Figure 8. Juxtaposition of return periods (in years) for extreme 5-day precipitation totals between control (CTRL, horizontal axis) and scenario (SCEN, vertical axis) time slices of RCM integrations. Both axes are log scaled. Results are for domain southern Scandinavia in winter. An example interpretation is as follows: In GKSS (short-dashed line) the domain mean 20-year return value in the SCEN integration is equal to the 100-year return value in the CTRL integration.

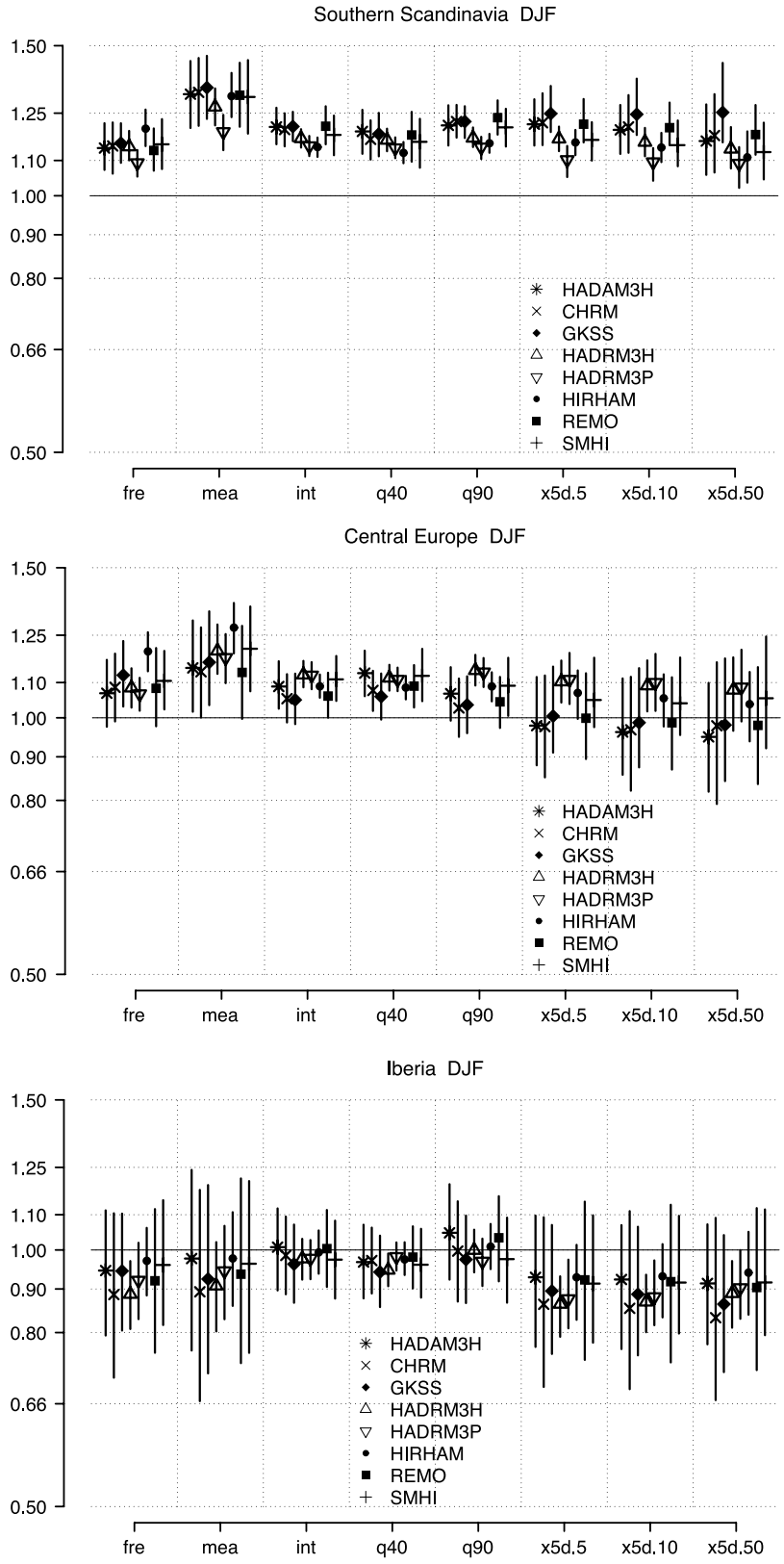

Figure 9. Simulated change (ratio SCEN/CTRL) in domain mean precipitation diagnostics for (top) southern Scandinavia, (middle) central Europe, and (bottom) Iberia in winter. See Table 1 for a description of diagnostics, Table 2 for model acronyms, and Figure 4 for domain definitions. Vertical bars are 95% bootstrap confidence intervals (see section 2.3). Vertical axes are log scaled.

extreme return values was examined by *Fowler and Hennessy* [1995].

[49] Note that frequency and intensity changes are measures of the frequency distribution of 1-day precipitation totals and hence the described scaling model is strictly a model for 1-day extremes. This is why we turn to consider 1-day extremes rather than 5-day extremes in the following, also for winter.

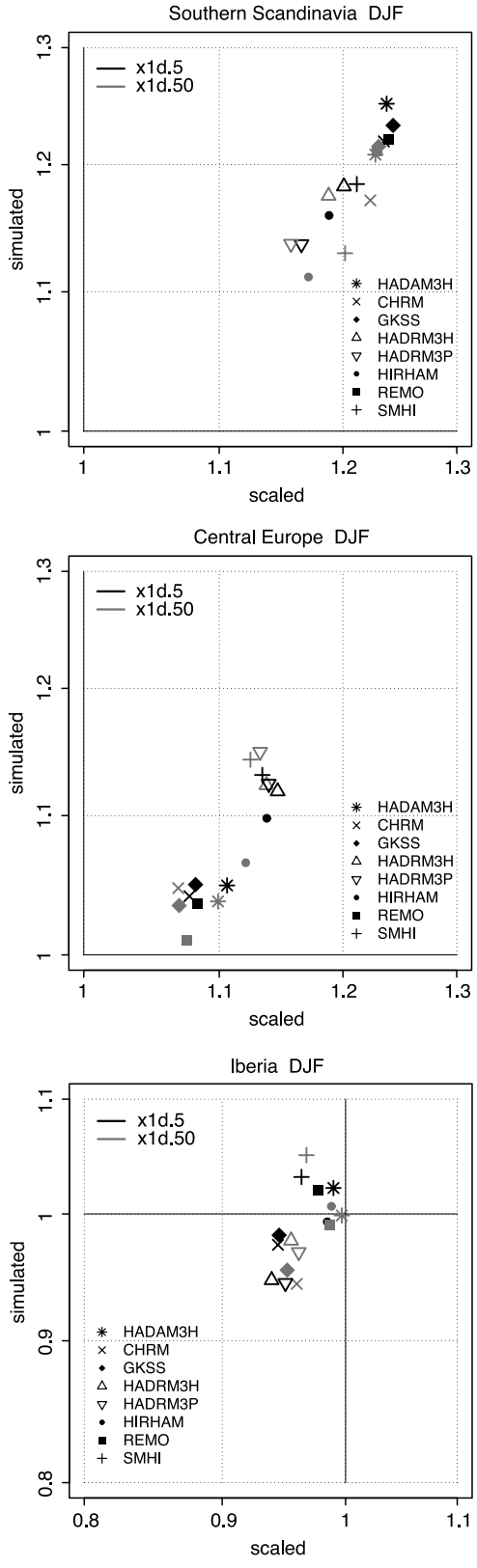

Figure 10. Simulated change in extreme return levels (ratio SCEN/CTRL, *y* axis) against expected change from a simple scaling of the CTRL distribution based on changes in wet day frequency and intensity (*x* axis; see text for details). Results are shown for x1d.5 (solid symbols) and x1d.50 (shaded symbols) in winter. Both axes are log scaled.

[50] Figure 10 compares the simulated change in return levels for winter with the change estimated from the simple scaling exercise. For both the 5-year and 50-year return levels the dots are closely aligned along the diagonal line for central Europe and southern Scandinavia. There are two implications from this. First, it appears that changes in precipitation extremes in central and northern Europe are dominated by the effect of changes in wet day frequency and intensity. Changes specific to extremes are of secondary importance in winter. Secondly, the scaling can accurately explain the variation of the change between the models. The intermodel variance explained by the scaling is larger than 90% for x1d.5 and larger than 66% for x1d.50 in both regions. This implies, in turn, that intermodel differences in the change of extremes (though small anyway) are due to, primarily, differences in how individual models respond in wet day frequency and intensity rather than in extremes per se. In fact, intensity change is the dominant factor at the tail (see Appendix A).

[51] As regards subdomain Iberia (Figure 10, bottom), the simulated change is still comparable to the change obtained from scaling. However, in this case it is the frequency decrease which appears to be responsible for the decrease of simulated extremes in most models because intensity changes are small, but the scatter is larger here (explained variance: 53% for x1d.5 and 25% for x1d.50) than for the other two regions, which can be understood from the larger estimation uncertainty found for this region (see Figure 9).

[52] The general picture emerging from these analyses for winter is that precipitation extremes increase over central and northern Europe primarily as a consequence of increases in wet day intensity and frequency. There is a high coherency in the change between the models. Intermodel differences arise primarily from differences in the change of wet day intensity and frequency and those are reasonably explained by interannual variations. The picture for summer is quite more complex as will be shown below.

5.2. Summer

[53] Figure 11 depicts the spatial distribution of the simulated change in the 5-year return value of 1-day precipitation intensity. As for winter, the continental-scale pattern of the change has some similarity between the models: There is a tendency for decreases over southern Europe and increases over northern and eastern Europe. (Note that some areas of southern Europe were masked out because of too few wet days. See section 2.1.) However, the details of the distribution are much more different between models than in winter: For example, HADRM3H simulates insignificant changes over central Europe and a decrease

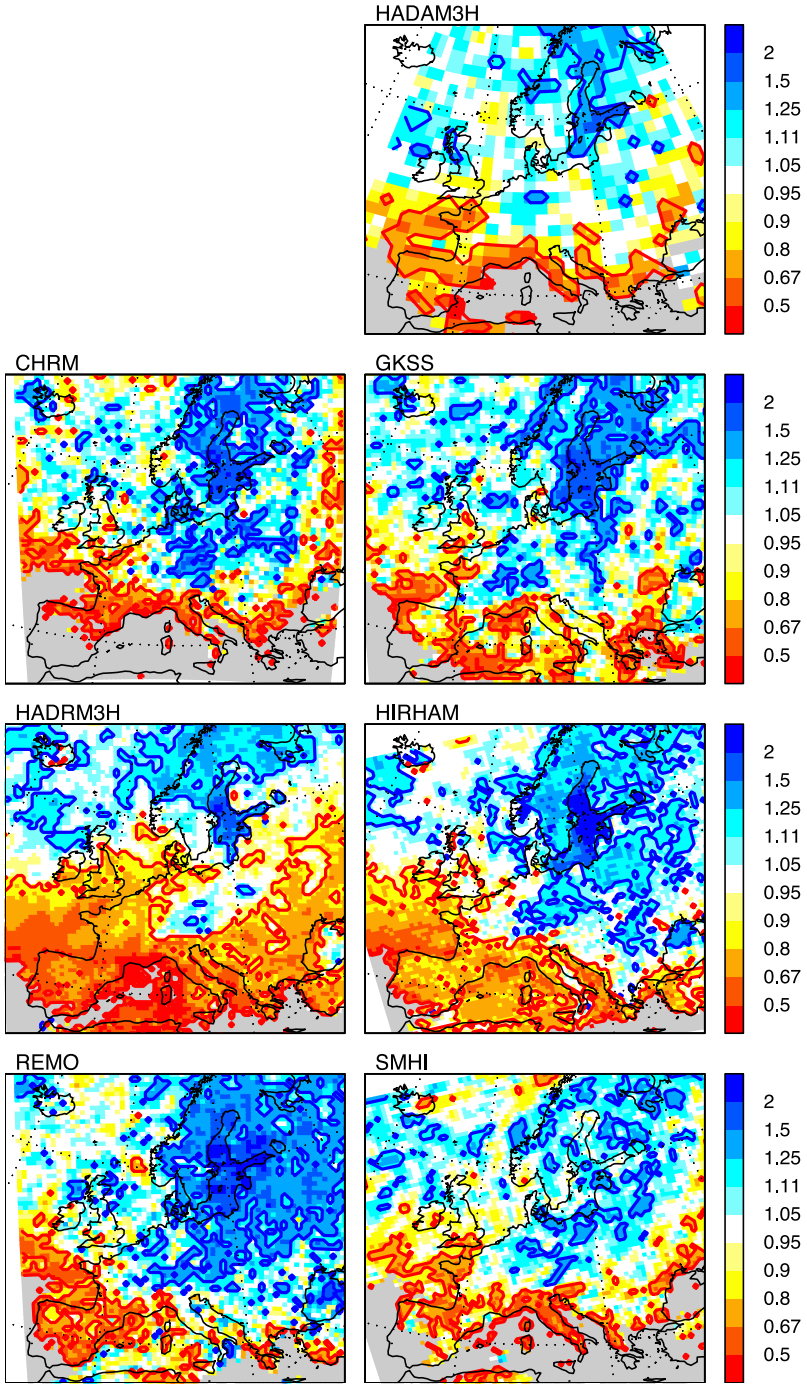

Figure 11. Same as Figure 7 but for the 1-day precipitation total (x1d.5) in summer (June–August). Shaded areas are for grid points where no extreme value analysis was feasible because of an insufficient number of rain days (see section 2.1).

over eastern Europe, whereas other models show a significant increase in these areas. Also, SMHI seems to have a generally smaller response compared to other models. Note that all models (except SMHI) exhibit a prominent increase over the Baltic Sea. This is an artifact resulting from an unrealistic increase in summer sea surface temperatures, which is due to the representation of the Baltic Sea as a lake in the coarse resolution of the coupled climate model. This does not affect SMHI because this model is coupled to a regional ocean model for the Baltic Sea [*Döscher et al.*, 2002], and hence does not specify ocean surface conditions from the GCM there.

[54] In contrast to winter, much larger intermodel differences are found in the simulated change of return values for summer (Table 4). In central Europe for the 5-year return value (x1d.5), for example, results range from a statistically significant decrease by 13% (HADRM3P) to a statistically significant increase by 21% (CHRM). Similarly large var-

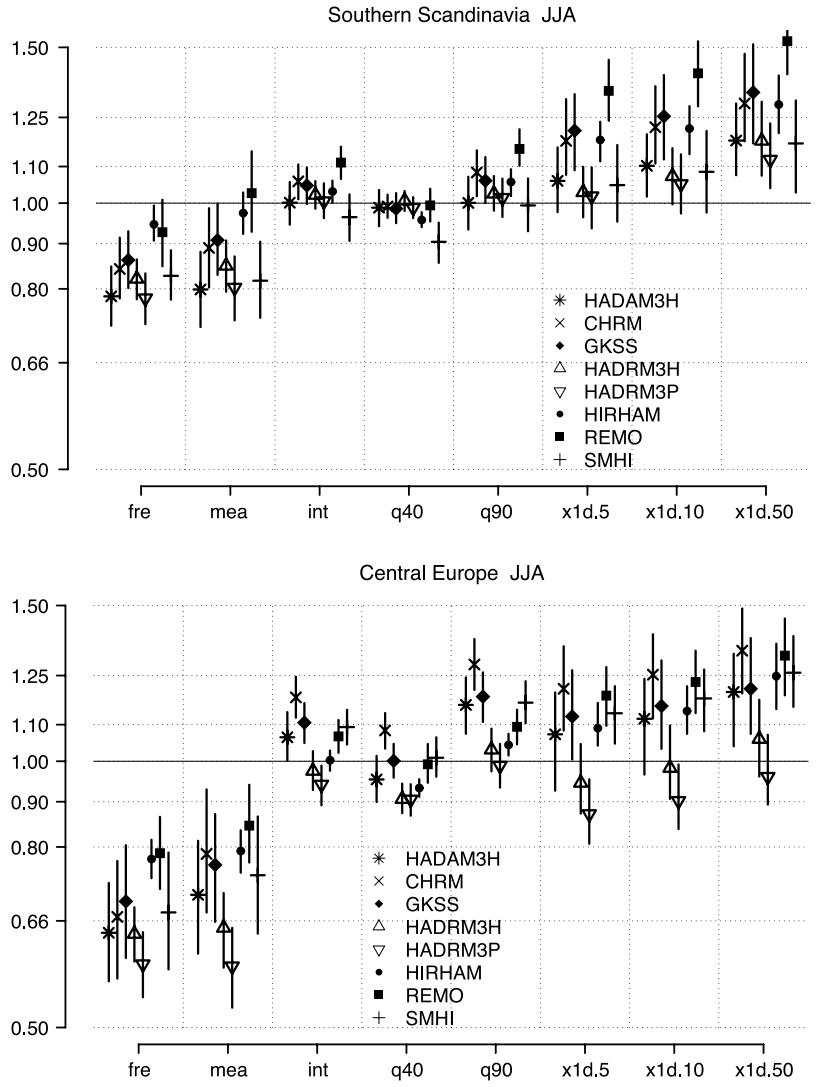

Figure 12. Same as Figure 9 but for summer. Results for Iberia are not reproduced because an extreme value analysis was not feasible at a large fraction of the grid points in this region in summer (see section 3.1).

iations are found for the basic diagnostics and moderate quantiles in southern Scandinavia and central Europe (Figure 12). The use of a different set of ensemble members does not explain these variations. SMHI and REMO, for example, show changes at opposite extremes in the model set for several diagnostics in southern Scandinavia although they are based on the same pair of ensemble members.

[55] Compared to winter, summer exhibits a much more complex structure of change across the precipitation distribution (Figure 12). In central Europe and southern Scandinavia, there is a decrease in wet day frequency, mostly statistically significant, but this is partly compensated by an increase of wet day intensity in many of the models. In all models, q40 decreases or changes very little, but there are progressively larger increases or smaller decreases as one moves toward the tail of the distribution. In fact, for both regions, it is the return value for the longest return period (50 years) that displays the most significant increase (except HADRM3H and HADRM3P in central Europe). Although the tendency for larger increases with longer return periods is a general behavior of all models, the critical frequency at which the decrease turns into an increase as one moves toward the tail, varies considerably between models (and also between the two regions). In central Europe, for example, HIRHAM changes sign at moderate precipitation intensities (between q40 and q90), but HADRM3H has increases only for very rare events with a recurrence of more than 10 years. These differences are evident even between models with comparable physical parameterizations (e.g., the GCM HADAM3H and HADRM3H).

[56] The pattern of an increasingly larger change for longer return period extremes does not necessarily imply that the summertime changes cannot be explained by the scaling model of equation (1). In Appendix A we illustrate that such a behavior could result from a decrease in wet day frequency combined with an increase in intensity, which is indeed observed in the models for southern Scandinavia and central Europe; however, more insight can be gained when the simple scaling exercise of the previous subsection is applied quantitatively to the results in summer. Figure 13

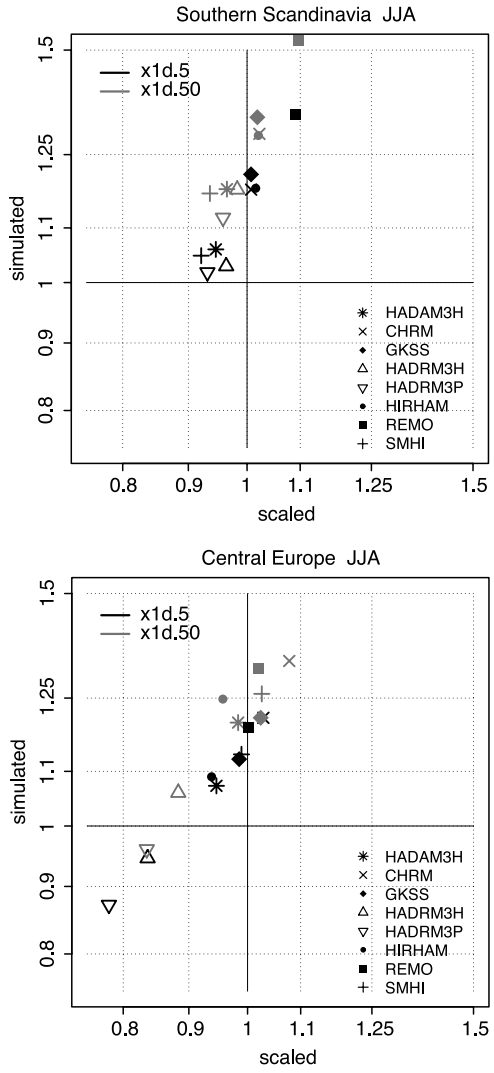

Figure 13. Same as Figure 10 but for summer. Both axes are log scaled. Note the larger range compared to Figure 10.

displays the results. First, all symbols are located well above the diagonal line in clear contrast to winter (Figure 10). Second, the symbols for the same return period are still arranged on a line. The implications are twofold.

[57] First, the simulated changes in wet day frequency and intensity cannot explain the magnitude of the simulated change in extremes. They would suggest larger decreases or smaller increases than those simulated by the models. In the simulations, there appears to be a process which is specific to extreme events and which contributes an increase that is superimposed to the change extrapolated from the change in average events. The tail-specific component of the change is very coherent between models, as is implied by the systematic offset of symbols from the diagonal. The offset is larger for x1d.50 than for x1d.5 suggesting that the component is progressive with more rare extremes. This is also evident from the fact that the connecting lines between x1d.5 and x1d.50 symbols of the same model have a steeper slope than 1 for all models.

[58] Second, even though not explaining the magnitude of change, the model specific changes in wet day frequency and intensity do explain a large fraction of the intermodel variance, also in summer. R^2 values for all scatter plots in Figure 13 exceed 0.9. Hence the large difference in the response for extremes comes from differences in the way the models simulate changes in wet day frequency and intensity (i.e., the change in average events), rather than the tail-specific component of the change.

[59] In summary, for summer, there is a much larger variation in the change of precipitation extremes between the RCMs than in winter. All models show a tendency toward larger increases or smaller decreases (depending on the model) with more and more extreme events. This is primarily due to a component of change affecting extremes more than average events. This component is fairly coherent between the models. Model differences are more due to differences in the change simulated in average events, particularly the change in wet day frequency and intensity.

5.3. Transition Seasons

[60] Changes in 1-day precipitation extremes show a very similar continental-scale pattern in spring and in autumn (not shown). In both seasons x1d.5 increases over most parts of the continent, especially over the northern, central and eastern parts. An exception is the Iberian Peninsula where x1d.5 decreases in spring and changes marginally in autumn. Several models exhibit particularly large increases in autumn over the Mediterranean Sea and Italy. The magnitude of the increase over southern Scandinavia and central Europe is similar to that in winter and the coherence between models is similar or even better than in winter (see Table 4). As regards the variation of the change across the frequency distribution, both seasons tend to replicate the simple structure of change found previously for winter. However, there are individual models (e.g., CHRM and REMO in autumn) showing progressively larger increases at longer return periods in central Europe. More detailed analysis for the transition seasons suggests that the simple scaling model reasonably explains the simulated changes at the tail in spring in southern Scandinavia, but there is evidence for a tail-specific component of the change, similar to but much smaller than in summer, for all regions in autumn.

6. Conclusions

[61] In the present study we undertook an intercomparison of precipitation extremes as simulated by six different European regional climate models, all with comparable model settings and driven with boundary data from the same global climate model. An evaluation of the model simulations for present climate in the region of the European Alps shows that RCMs are capable of representing mesoscale spatial patterns in precipitation extremes that are not resolved by today's GCMs. However, model biases are large in some cases, in particular in summer. Even for rare extremes (5-year return values), these biases were nevertheless similar to or smaller than those for wet day intensity or mean precipitation. We conclude that there is no evidence from this evaluation for model errors that are specific to precipitation extremes and that are not evident in simpler, average diagnostics. Moreover, comparison to earlier evaluations of similar RCMs, but driven by reanalysis data [*Frei*

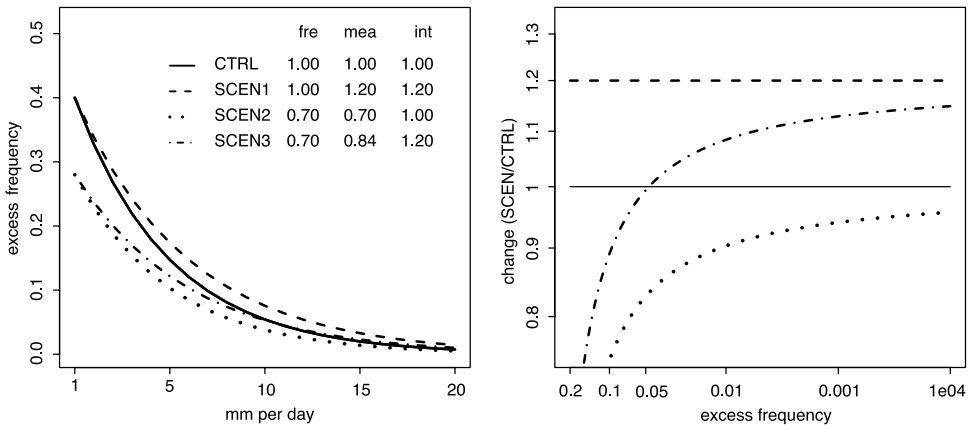

Figure A1. Illustration of the variations in the cumulative frequency distribution of daily precipitation resulting from three stipulated scaling scenarios. (a) Excess frequency as a function of threshold (upper tail cumulative frequency distribution). (b) Associated change in quantiles (SCEN/CTRL, log scale) as a function of excess frequency (log scale). The change in the 99.9% quantile (approximately the 2.7-year return value) is depicted at excess frequency 0.001. The inset in Figure A1a lists the stipulated changes (SCEN/CTRL) in wet day frequency (fre) and intensity (int) and the resulting change for mean precipitation (mea). The illustration is based on the exponential distribution family. This is a reproduction of a similar illustration given by *Fowler and Hennessy* [1995], but changes are expressed for quantiles.

et al., 2003], implies that errors inherited from the driving GCM were small and did not alter the RCM specific error characteristics, which, in retrospect, attests to the quality of the GCM's present-day climate.

[62] The simulated future change in European precipitation extremes shows a seasonally very distinct pattern: In winter, land regions north of about 45°N experience an increase in multiyear return values while the Mediterranean region experiences small changes with a general tendency toward decreases. Results are very consistent between the six RCMs, with the change in 5-year return values increasing by 0–11% in central Europe and by 10–22% in southern Scandinavia. The simulated increase of extremes is accurately explained by the increase in wet day intensity and frequency in a simple rescaling of the distribution for present climate.

[63] The increase in wintertime precipitation extremes is a robust feature in RCM climate change experiments over Europe. Versions of the RCMs considered in this study, but driven by different GCMs, yield changes very similar to those found in this study [*Durman et al.*, 2001; *Räisänen et al.*, 2004]. Also, the simulated response in winter qualitatively conforms to the observed trends in heavy precipitation over Europe, which shows an increase in winter primarily north of 45°N [e.g., *Klein Tank and Können*, 2003; *Fowler and Kilsby*, 2003a, 2003b; *Haylock and Goodess*, 2004; *Brunetti et al.*, 2004; *Schmidli and Frei*, 2005]. These similarities are worth noting, but it is premature to infer the detection of an anthropogenic influence on heavy precipitation in Europe [see also *Kiktev et al.*, 2003, 2004; *Hegerl et al.*, 2004].

[64] In summer the character of change is more complex: The larger-scale pattern shows a gradient from increases in northern Scandinavia to decreases in the Mediterranean region and this is fairly similar between models, but the transition across the continent differs between models and the magnitude of the change in the 5-year return value varies considerably (−13% to +21% for central Europe and +2 to +34% for southern Scandinavia). The large model differences are well explained by differences in the change of average precipitation events as represented by wet day intensity and frequency. This suggests that it is primarily the response in the basic intensity and occurrence process of precipitation where models differ, and not the particular response in the extremes themselves. The prominent role of physical parameterizations (e.g., convection, land-surface atmosphere exchange, radiation, and clouds) may explain the large model spread in summer compared to winter where large-scale circulation exerts a stronger control [e.g., *Noguer et al.*, 1998; *Schär et al.*, 1999].

[65] However, the models simulate a larger increase or smaller decrease of extremes than would have been anticipated from the simulated change in wet day intensity and frequency alone. The change in summer is therefore also governed by a factor affecting the frequency distribution more fundamentally and specifically at the tail. This factor tends to increase extreme quantiles in the simulation for future climate, independently of the sign of the total change in the quantiles. This tail-specific component is seen consistently in all RCMs and its magnitude is considerable, capable of reversing a decrease that would be expected from changes in mean conditions alone, into an increase.

[66] The present analysis offers a more in depth statistical interpretation of results from previous studies on the future change of European summer precipitation extremes. In their RCM experiments, *Christensen and Christensen* [2003, 2004] and *Pal et al.* [2004] found increases in high precipitation quantiles in central Europe although mean precipitation was simulated to decrease. In this study, for central Europe we find an increase in five but a decrease in 2 models. In principle an increase of extremes would be possible even if the change at the tail was determined by the change in average conditions alone (see Appendix A). At sufficiently high return values an increase in wet day

intensity always dominates a decrease in wet day frequency, even if the frequency decrease is larger than the intensity increase, i.e., when mean precipitation decreases. The present analysis suggests that this simple picture is not a sufficient explanation for the model results. The change in summer extremes indeed reflects a nontrivial change at the tail of the distribution. This excessive response for extremes is found consistently in all RCMs, even in those two models where extreme return values actually decrease. Also, the same behavior is noted further north in Scandinavia, where a response more similar to winter could have been expected. However, there is a large intermodel difference in the sign and magnitude of the change at a particular frequency level (return period), which is primarily related to the different responses in average conditions, and contributes to considerable uncertainty about the future change in European summer precipitation extremes.

[67] Clearly, more research will be needed to understand the physical nature of the tail-specific response and the reasons for the different model responses in summer. Also, tests with more complex scaling models could shed more light in the statistical nature of the peculiar change in summertime precipitation pdfs. From the point of view of scenarios, the present analysis suggests that the formulation of regional models (e.g., the parameterization) contributes significantly to the uncertainty in scenarios of summer precipitation extremes. It is therefore not a waste of resources if multimodel ensemble systems, devoted to estimating scenario uncertainties, include a set of RCMs nested into the same GCM, alongside the nesting of RCMs in several different GCMs.

Appendix A

[68] *Fowler and Hennessy* [1995] illustrated that changes in wet day frequency (fre) and intensity (int) in combination with the scaling model of section 5 have remarkably different effects on the frequency of extreme precipitation events. For a typical frequency distribution of daily precipitation a change in wet day intensity results in increasingly larger changes in excess frequency at larger thresholds. In contrast, the change in excess frequency from a change in wet day frequency is independent of the threshold. This implies that a nonzero change in wet day intensity dominates a change in frequency for sufficiently large thresholds.

[69] Figure A1 illustrates this behavior but with respect to the change in quantiles. For simplicity, the illustration is based on the exponential distribution as an example for a frequency distribution of daily precipitation (CTRL in Figure A1a), but the behavior is not depending on details of the distribution function. Obviously, an increase in int (e.g., by 20%, SCEN1, dashed line in Figure A1) results in a similar increase for all quantiles. On the other hand, a decrease in fre (e.g., by 30%, SCEN2, Figure A1, dotted line) results in a larger decrease in light or moderate compared to large precipitation quantiles. Finally, a combination of a decrease in fre and an increase in int (SCEN3, Figure A1, dash-dotted line) would yield a change, which is dominated by the sign of the fre change at light quantiles and by the sign and magnitude of the int change at large quantiles. Note that SCEN3 can explain qualitatively that a decrease in mean precipitation can go along with an increase of extreme quantiles; however, the results of section 5, show that the combination of fre and int changes cannot explain quantitatively the simulated change of extremes in summer.

[70] **Acknowledgments.** We are grateful to Christopher A. T. Ferro, Christoph Schär, and David B. Stephensen for useful discussions on the subject and results of this study and to Ole B. Christensen for setting up the PRUDENCE database from which the RCM data were retrieved. We also thank three anonymous reviewers whose comments helped to improve our earlier manuscript. The following institutes have kindly provided access to climate model data and to daily precipitation data in the Alps: DMI, Copenhagen, Denmark; GKSS, Geesthacht, Germany; Hadley Centre U.K. Met Office, Exeter, United Kingdom; MPI, Hamburg, Germany; SMHI, Norrköpping, Sweden; DWD, Offenbach, Germany; Hydrographisches Zentralbüro, Vienna, Austria; ZAMG, Vienna, Austria; Météo France, Toulouse, France; UCEA, Rome, Italy; MeteoSwiss, Zürich, Switzerland; SIMN, Rome, Italy; Meteorological Service, Zagreb, Croatia; and Hydrometeorological Institute, Ljubljana, Slovenia. This research was supported by the 5th Framework Program of the European Union (projects STARDEX, contract EVK2-2001-00115, and PRUDENCE, contract EVK2-CT200100132) and by the Swiss Ministry for Education and Science (BBW contract 01.0265-2). Additional support was provided by the Swiss National Science Foundation (NCCR Climate). C. F. acknowledges additional support by MeteoSwiss, Zürich.

References

Allen, M. R., and W. J. Ingram (2002), Constraints on future changes in climate and the hydrologic cycle, *Nature*, *419*, 224–232.

Anderson, C. J., et al. (2003), Hydrological processes in regional climate model simulations of the central United States flood of June–July 1993, *J. Hydrometeorol.*, *4*, 584–598.

Arora, V. K., and G. J. Boer (2001), Effects of simulated climate change on the hydrology of major river basins, *J. Geophys. Res.*, *106*, 3335–3348.

Booij, M. J. (2002), Extreme daily precipitation in western Europe with climate change at appropriate spatial scales, *Int. J. Climatol.*, *22*, 69–85.

Brunetti, M., M. Maugeri, F. Monti, and T. Nanni (2004), Changes in daily precipitation frequency and distribution in Italy over the last 120 years, *J. Geophys. Res.*, *109*, D05102, doi:10.1029/2003JD004296.

Christensen, J. H., and O. B. Christensen (2003), Severe summertime flooding in Europe, *Nature*, *421*, 805–806.

Christensen, J. H., and O. B. Christensen (2004), Intensification of extreme European summer precipitation in a warmer climate, *Global Planet. Change*, *44*, 107–117.

Christensen, J. H., O. B. Christensen, P. Lopez, E. Van Meljgaard, and M. Botzet (1996), The HIRHAM4 regional atmospheric climate model, *Sci. Rep. 96-4*, 51 pp., Dan. Meteorol. Inst., Copenhagen.

Christensen, J. H., T. R. Carter, and M. Rummukainen (2006), Evaluating the performance and utility of regional climate models: The PRUDENCE project, *Clim. Change*, in press.

Coles, S. (2001), *An Introduction to Statistical Modeling of Extreme Values*, 208 pp., Springer, New York.

Cubasch, U., et al. (2001), Projections of future climate change, in *Climate Change 2001: The Scientific Basis*, *Contribution of Working Group I to the Third Assessment Report of the Intergovernmental Panel on Climate Change*, edited by J. T. Houghton et al., pp. 525–582, Cambridge Univ. Press, New York.

De Elia, R., and R. Laprise (2003), Distribution-oriented verification of limited-area model forecasts in a perfect-model framework, *Mon. Weather Rev.*, *131*, 2492–2509.

Denis, B., R. Laprise, D. Caya, and J. Côté (2002), Downscaling ability of one-way nested regional climate models: The Big-Brother experiment, *Clim. Dyn.*, *18*, 627–646.

Déqué, M., et al. (2005), An intercomparison of regional climate models for Europe: Assessing uncertainties in model projections, *Clim. Dyn.*, *25*, 653–670.

Döscher, R., U. Willén, C. Jones, A. Rutgersson, H. E. M. Meier, U. Hansson, and L. P. Graham (2002), The development of the coupled regional ocean-atmosphere model RCAO, *Boreal Environ. Res.*, *7*, 183–192.

Durman, C. F., J. M. Gregory, D. C. Hassell, R. G. Jones, and J. M. Murphy (2001), A comparison of extreme European daily precipitation simulated by a global and a regional climate model for present and future climates, *Q. J. R. Meteorol. Soc.*, *127*, 1005–1015.

Ekström, M., H. J. Fowler, C. G. Kilsby, and P. D. Jones (2005), New estimates of future changes in extreme rainfall across the UK using

regional climate model integrations. 2. Future estimates and use in impact studies, *J. Hydrol.*, *300*, 234–251.
Fisher, R. A., and L. H. C. Tippett (1928), Limiting forms of the frequency distribution of the largest or smallest members of a sample, *Proc. Cambridge Philos. Soc.*, *24*, 180–190.
Fowler, A. M., and K. J. Hennessy (1995), Potential impacts of global warming on the frequency and magnitude of heavy precipitation, *Nat. Hazards*, *11*, 282–303.
Fowler, H. J., and C. G. Kilsby (2003a), A regional frequency analysis of United Kingdom extreme rainfall from 1961 to 2000, *Int. J. Climatol.*, *23*, 1313–1334.
Fowler, H. J., and C. G. Kilsby (2003b), Implications of changes in seasonal and annual extreme rainfall, *Geophys. Res. Lett.*, *30*(13), 1720, doi:10.1029/2003GL017327.
Fowler, H. J., M. Ekström, C. G. Kilsby, and P. D. Jones (2005), New estimates of future changes in extreme rainfall across the UK using regional climate model integrations: 1. Assessment of control climate, *J. Hydrol.*, *300*, 212–233.
Frei, C., and C. Schär (1998), A precipitation climatology of the Alps from high-resolution rain-gauge observations, *Int. J. Climatol.*, *18*, 873–900.
Frei, C., C. Schär, D. Lüthi, and H. C. Davies (1998), Heavy precipitation processes in a warmer climate, *Geophys. Res. Lett.*, *25*, 1431–1434.
Frei, C., J. H. Christensen, M. Déqué, D. Jacob, R. G. Jones, and P. L. Vidale (2003), Daily precipitation statistics in regional climate models: Evaluation and intercomparison for the European Alps, *J. Geophys. Res.*, *108*(D3), 4124, doi:10.1029/2002JD002287.
Gnedenko, B. (1943), Sur la distribution limite du terme maximum d'une série aléatoire, *Ann. Math.*, *44*, 423–453.
Goodess, C. M. (2003), Statistical and Regional dynamical Downscaling of Extremes for European regions: STARDEX, *EGGS*, *6*.
Gordon, C., C. Cooper, C. A. Senior, H. Banks, H. M. Gregory, T. C. Johns, J. F. B. Mitchell, and R. A. Wood (2000), The simulation of SST, sea ice extent and ocean heat transports in a version of the Hadley Centre coupled model without flux adjustments, *Clim. Dyn.*, *16*, 147–168.
Groisman, P. Y., and D. R. Legates (1994), The accuracy of United States precipitation data, *Bull. Am. Meteorol. Soc.*, *75*, 215–227.
Groisman, P. Y. A., et al. (1999), Changes in the probability of heavy precipitation: Important indicators of climatic change, *Clim. Change*, *42*, 243–283.
Gumbel, E. J. (1958), *Statistics of Extremes*, 375 pp., Columbia Univ. Press, New York.
Hagemann, S., M. Botzet, L. Dümenil, and B. Machenhauer (1999), Derivation of global GCM boundary conditions for 1 km land use satellite data, *Rep. 2189*, Max-Planck Inst. für Meteorol., Hamburg, Germany.
Hagemann, S., M. Botzet, and B. Machenhauer (2001), The summer drying problem over south-eastern Europe: Sensitivity of the limited area model HIRHAM4 to improvements in physical parameterization and resolutioin, *Phys. Chem. Earth, Part B*, *26*, 391–396.
Hagemann, S., B. Machenhauer, R. Jones, O. B. Christensen, M. Déqué, D. Jacob, and P. L. Vidale (2004), Evaluation of water and energy budgets in regional climate models applied over Europe, *Clim. Dyn.*, *23*, 547–567.
Haylock, M. R., and C. M. Goodess (2004), Interannual variability of extreme European winter rainfall and links with mean large-scale circulation, *Int. J. Climatol.*, *24*, 759–776.
Hegerl, G. C., F. W. Zwiers, P. A. Stott, and V. V. Kharin (2004), Detectability of anthropogenic changes in temperature and precipitation extremes, *J. Clim.*, *17*, 3683–3700.
Hirschi, M., S. I. Seneviratne, and C. Schär (2006), Seasonal variations in terrestrial water storage for major midlatitude river basins, *J. Hydrometeorol.*, in press.
Hosking, J. R. M. (1985), Algorithm AS 215: Maximum-likelihood estimation of the parameter of the generalized extreme-value distribution, *Appl. Stat.*, *34*, 301–310.
Hosking, J. R. M. (1990), L-moments: Analysis and estimation of distributions using linear combinations of order statistics, *J. R. Stat. Soc., Ser. B*, *52*, 105–124.
Hosking, J. R. M. (1992), Moments or L-moments? An example comparing two measures of distributional shape, *Am. Stat.*, *46*, 186–189.
Hosking, J. R. M., and J. R. Wallis (1993), Some statistics useful in regional frequency analysis, *Water Resour. Res.*, *29*, 271–281.
Huntingford, C., R. G. Jones, C. Prudhomme, R. Lamb, H. H. C. Gash, and D. A. Jones (2003), Regional climate-model predictions of extreme rainfall for a changing climate, *Q. J. R. Meteorol. Soc.*, *129*, 1607–1621.
Jacob, D. (2001), A note to the simulation of the annual and inter-annual variability of the water budget over the Baltic Sea drainage basin, *Meteorol. Atmos. Phys.*, *77*, 66–73.
Johns, T. C., et al. (2003), Anthropogenic climate change for 1860 to 2100 simulated with the HadCM3 model under updated emission scenarios, *Clim. Dyn.*, *20*, 583–612.
Jones, C. (2001), A brief description of RCA2, Rossby Centre Atmosphere Model version 2, *SWECLIM Newsl. 11*, pp. 9–14, Swed. Meteorol. and Hydrol. Inst., Norrköping. (Available at http://www.smhi.se/sgn0106/rossby/sweclim/newsletter/newsletter_11.pdf)
Jones, P. D., and P. A. Reid (2001), Assessing future changes in extreme precipitation over Britain using regional climate model integrations, *Int. J. Climatol.*, *21*, 1337–1356.
Jones, R. G., J. M. Murphy, and M. Noguer (1995), Simulation of climate change over Europe using a nested regional-climate model. I: Assessment of control climate, including sensitivity to location of lateral boundaries, *Q. J. R. Meteorol. Soc.*, *121*, 1413–1449.
Jones, R. G., J. M. Murphy, M. Noguer, and A. B. Keen (1997), Simulation of climate change over Europe using a nested regional-climate model: II. Comparison of driving and regional model responses to a doubling of carbon dioxide, *Q. J. R. Meteorol. Soc.*, *123*, 265–292.
Jones, R. G., M. Noguer, D. C. Hassell, D. Hudson, S. S. Wilson, G. J. Jenkins and J. F. B. Mitchell (2004), Generating high resolution climate change scenarios using PRECIS, report, 35 pp., Hadley Cent., Met Off., Exeter, U. K.
Katz, R. W., and J. G. Acero (1994), Sensitivity of extreme precipitation events, *Int. J. Climatol.*, *14*, 985–999.
Katz, R. W., M. B. Parlange, and P. Naveau (2002), Statistics of extremes in hydrology, *Adv. Water Resour.*, *25*, 1287–1304.
Kharin, V. V., and F. W. Zwiers (2000), Changes in the extremes in an ensemble of transient climate simulations with a coupled atmosphere-ocean GCM, *J. Clim.*, *13*, 3760–3788.
Kiktev, D., D. M. H. Sexton, L. Alexander, and C.K. Folland (2003), Comparison of modeled and observed trends in indices of daily climate extremes, *J. Clim.*, *16*, 3560–3571.
Kiktev, D., D. M. H. Sexton, L. Alexander, and C. K. Folland (2004), Corrigendum: Comparison of modeled and observed trends in indices of daily climate extremes, *J. Clim.*, *17*, 2489.
Klein Tank, A. M. G., and G. P. Können (2003), Trends in indices of daily temperature and precipitation extremes in Europe, 1946–1999, *J. Clim.*, *16*, 3665–3680.
Lüthi, D., A. Cress, C. Frei, and C. Schär (1996), Interannual variability and regional climate simulations, *Theor. Appl. Climatol.*, *53*, 185–209.
Martins, E. S., and J. R. Stedinger (2000), Generalized maximum-likelihood generalized extreme-value quantile estimators for hydrologic data, *Water Resour. Res.*, *36*, 737–744.
Meier, H. E. M., R. Döscher, A. C. Coward, and J. Nycander (1999), Rossby Centre regional ocean climate mode: Model description (version 1.0) and first results from the hindcast period 1992/1993, *SMHI Rep. Oceanogr. 26*, 102 pp., Swed. Meteorol. and Hydrol. Inst., Norrköping.
Nakicenovic, N., et al. (2000), *Special Report on Emissions Scenarios: A Special Report of Working Group III for the Integovernmental Panel on Climate Change*, 599 pp., Cambridge Univ. Press, New York.
Neff, E. L. (1977), How much rain does a rain gage gage?, *J. Hydrol.*, *35*, 213–220.
Noguer, M., R. G. Jones, and J. M. Murphy (1998), Sources of systematic errors in the climatology of a regional climate model over Europe, *Clim. Dyn.*, *14*, 691–712.
Osborn, T. J., and M. Hulme (1997), Development of a relationship between station and grid-box rainday frequencies for climate model evaluation, *J. Clim.*, *10*, 1885–1908.
Pal, J. S., F. Giorgi, and X. Bi (2004), Consistency of recent European summer precipitation trends and extremes with future regional climate projections, *Geophys. Res. Lett.*, *31*, L13202, doi:10.1029/2004GL019836.
Palmer, T. N., and J. Räisänen (2002), Quantifying the risk of extreme seasonal precipitation events in a changing climate, *Nature*, *415*, 512–514.
Palutikof, J. P., B. B. Brabson, D. H. Lister, and S. T. Adcock (1999), A review of methods to calculate extreme wind speeds, *Meteorol. Appl.*, *6*, 119–132.
Pope, D. V, M. Gallani, R. Rowntree, and A. Stratton (2000), The impact of new physical parameterizations in the Hadley Centre climate model: HadAM3, *Clim. Dyn.*, *16*, 123–146.
Räisänen, J., U. Hannson, A. Ullerstig, R. Döscher, L. P. Graham, C. Jones, H. E. M. Meier, P. Samuelsson, and U. Willén (2004), European climate in the late twenty-first century: Regional simulations with two global models and two forcing scenarios, *Clim. Dyn.*, *22*, 13–31.
Roeckner, E., K. Arpe, L. Bengtsson, M. Christoph, M. Claussen, L. Dümenil, M. Esch, M. Giorgetta, U. Schlese, and U. Schulzweida (1996), The atmospheric general circulation model ECHAM-4: Model description and simulation of present-day climate, *Rep. 218*, 90 pp., Max-Planck Inst. für Meteorol., Hamburg, Germany.
Schär, C., D. Lüthi, U. Beyerle, and E. Heise (1999), The soil-precipitation feedback: A process study with a regional climate model, *J. Clim.*, *12*, 722–741.

Schär, C., P. L. Vidale, D. Lüthi, C. Frei, C. Häberli, M. A. Liniger, and C. Appenzeller (2004), The role of increasing temperature variability in European summer heatwaves, *Nature*, *427*, 332–336.

Schmidli, J., and C. Frei (2005), Trends of heavy precipitation and wet and dry spells in Switzerland during the 20th century, *Int. J. Climatol.*, *25*, 753–771.

Schwarb, M., C. Daly, C. Frei, and C. Schär (2001), Mean annual and seasonal precipitation in the European Alps 1971–1990, in *Hydrological Atlas of Switzerland*, plates 2.6, 2.7, Landeshydrol. und Geol., Bern.

Semenov, V. A., and L. Bengtsson (2002), Secular trend in daily precipitation characteristics: Greenhouse gas simulation with a coupled AOGCM, *Clim. Dyn.*, *19*, 123–140.

Semmler, T., and D. Jacob (2004), Modeling extreme precipitation events—A climate change simulation for Europe, *Global Planet. Change*, *44*, 119–127.

Sevruk, B. (1985), Systematischer Niederschlagsmessfehler in der Schweiz, in *Der Niederschlag in der Schweiz*, edited by B. Sevruk, *Beitr. Geol. Schweiz Hydrol.*, *31*, 65–75.

Shepard, D. S. (1984), Computer mapping: The SYMAP interpolation algorithm, in *Spatial Statistics and Models*, edited by G. L. Gaile and C. J. Willmott, pp. 133–145, Springer, New York.

Steppeler, J., G. Doms, U. Schättler, H. W. Bitzer, A. Gassmann, U. Damrath, and G. Gregoric (2003), Meso-gamma scale forecasts using the nonhydrostatic model LM, *Meteorol. Atmos. Phys.*, *82*, 75–96.

Trenberth, K. E. (1999), Conceptual framework for changes of extremes of the hydrological cycle with climate change, *Clim. Change*, *42*, 327–339.

Trenberth, K. E., A. Dai, R. M. Rasmussen, and D. B. Parsons (2003), The changing character of precipitation, *Bull. Am. Meteorol. Soc.*, *84*, 1205–1217.

Vidale, P. L., D. Lüthi, C. Frei, S. Seneviratne, and C. Schär (2003), Predictability and uncertainty in a regional climate model, *J. Geophys. Res.*, *108*(D18), 4586, doi:10.1029/2002JD002810.

Voss, R., W. May, and E. Roeckner (2002), Enhanced resolution modeling study on anthropogenic climate change: Changes in extremes of the hydrological cycle, *Int. J. Climatol.*, *22*, 755–777.

Watterson, I. G., and M. R. Dix (2003), Simulated changes due to global warming in daily precipitation means and extremes and their interpretation using the gamma distribution, *J. Geophys. Res.*, *108*(D13), 4379, doi:10.1029/2002JD002928.

Wehner, M. F. (2004), Predicted twenty-first-century changes in seasonal extreme precipitation events in the parallel climate model, *J. Clim.*, *17*, 4281–4290.

Widmann, M., and C. S. Bretherton (2000), Validation of mesoscale precipitation in the NCEP reanalysis using a new grid point data set for the northwestern US, *J. Clim.*, *13*, 1936–1950.

Wigley, T. M. L., and S. C. B. Raper (2001), Interpretation of high projections for global-mean warming, *Science*, *293*, 451–454.

Wilby, R. L., T. M. L. Wigley, D. Conway, P. D. Jones, and B. C. Hewitson (1998), Statistical downscaling of general circulation model output: A comparison of methods, *Water Resour. Res.*, *34*, 2995–3008.

Wilks, D. S. (1997), Resampling hypothesis tests for autocorrelated fields, *J. Clim.*, *10*, 65–82.

Woth, K., R. Weisse, and H. von Storch (2005), Climate change and North Sea storm surge extremes: An ensemble study of storm surge extremes expected in a changed climate projected by four different regional climate models, *Ocean Dyn.*, doi:10.1007/s10236-005-0024-3.

Zwiers, F. W., and V. V. Kharin (1998), Changes in the extremes of the climate simulated by CC GCM2 under CO_2 doubling, *J. Clim.*, *11*, 2200–2222.

C. Frei, Federal Office of Meteorology and Climatology (MeteoSwiss), Krähbühlstrasse 58, CH-8044 Zürich, Switzerland. (christoph.frei@meteoswiss.ch)

S. Fukutome, Institute of Terrestrial Ecology, ETH, Universitätstrasse 16, CH-8092 Zürich, Switzerland.

J. Schmidli, Institute for Atmospheric and Climate Science, ETH, Universitätstrasse 16, CH-8092 Zürich, Switzerland.

R. Schöll, Institute for Human-Environment Systems, ETH, Universitätstrasse 16, CH-8092 Zürich, Switzerland.

P. L. Vidale, CGAM, Department of Meteorology, University of Reading, PO Box 243, Reading RG6 6BB, UK.